UNCLASSIFIED
SECURITY CLASSIFICATION OF THIS PAGE

MASTER COPY

FOR REPRODUCTION PURPOSES

REPORT DOCUMENTATION PAGE

1a. REPORT SECURITY CLASSIFICATION: Unclassified	1b. RESTRICTIVE MARKINGS
2a. SECURITY CLASSIFICATION AUTHORITY	3. DISTRIBUTION/AVAILABILITY OF REPORT: Approved for public release; distribution unlimited.
2b. DECLASSIFICATION/DOWNGRADING SCHEDULE	
4. PERFORMING ORGANIZATION REPORT NUMBER(S)	5. MONITORING ORGANIZATION REPORT NUMBER(S): ARO 22612.11-EG
6a. NAME OF PERFORMING ORGANIZATION: University of California, San Diego	6b. OFFICE SYMBOL (If applicable)
6c. ADDRESS (City, State, and ZIP Code): Dept of Applied Mechanics & Engineering Sci 9500 Gilman Drive, 0411 La Jolla, California 92093-0411	7a. NAME OF MONITORING ORGANIZATION: U. S. Army Research Office
	7b. ADDRESS (City, State, and ZIP Code): P. O. Box 12211 Research Triangle Park, NC 27709-2211
8a. NAME OF FUNDING/SPONSORING ORGANIZATION: U. S. Army Research Office	8b. OFFICE SYMBOL (If applicable)
8c. ADDRESS (City, State, and ZIP Code): P. O. Box 12211 Research Triangle Park, NC 27709-2211	9. PROCUREMENT INSTRUMENT IDENTIFICATION NUMBER: DAAL03-86-K-0001
	10. SOURCE OF FUNDING NUMBERS: PROGRAM ELEMENT NO. / PROJECT NO. / TASK NO. / WORK UNIT ACCESSION NO

11. TITLE (Include Security Classification)

MECHANISMS OF COMBUSTION OF HYDROCARBON/ALCOHOL FUEL BLENDS

12. PERSONAL AUTHOR(S)
Kalyanasundaram Seshadri

13a. TYPE OF REPORT	13b. TIME COVERED	14. DATE OF REPORT (Year, Month, Day)	15. PAGE COUNT
Final Technical	FROM 10/15/85 TO 2/28/81	November 1, 1990	88

16. SUPPLEMENTARY NOTATION
The view, opinions and/or findings contained in this report are those of the author(s) and should not be construed as an official Department of the Army position, policy, or decision, unless so designated by other documentation.

17. COSATI CODES			18. SUBJECT TERMS (Continue on reverse if necessary and identify by block number)
FIELD	GROUP	SUB-GROUP	

19. ABSTRACT (Continue on reverse if necessary and identify by block number)

The principal objective of this research is to obtain an improved understanding of the structure of laminar flames burning hydrocarbon fuels, alcohol fuels, and blends of hydrocarbon and alcohol fuels. This work attempts to support the U. S. Army's research and development programs in alternative fuels. Since, there is convincing evidence that turbulent reacting flows can be modelled as statistical ensemble of laminar flamelets, an experimental, numerical and analytical study was undertaken to clarify the structure and mechanisms of extinction of laminar diffusion flamelets, laminar premixed flamelets and laminar partially premixed flamelets.

20. DISTRIBUTION/AVAILABILITY OF ABSTRACT: ☐ UNCLASSIFIED/UNLIMITED ☒ SAME AS RPT. ☐ DTIC USERS	21. ABSTRACT SECURITY CLASSIFICATION: Unclassified
22a. NAME OF RESPONSIBLE INDIVIDUAL: Kalyanasundaram Seshadri	22b. TELEPHONE (Include Area Code): (619) 534-4876 / 22c. OFFICE SYMBOL

DD FORM 1473, 84 MAR — 83 APR edition may be used until exhausted. All other editions are obsolete.

SECURITY CLASSIFICATION OF THIS PAGE
UNCLASSIFIED

19.

Results of the study on diffusion flames burning hydrocarbon and alcohol fuel show that the basic structure of these flames are essentially similar and can be modelled by use of four overall reactions. Only one of these overall reactions is specific to the fuel being considered, while the other three reactions are those which describe the oxidation of H_2 and CO to H_2O and CO_2. It was found that chemical reactions occur in roughly two distinct layers which are termed the inner layer and the oxidation layer. In the inner layer the fuel is attacked by the radicals to form H_2 and CO, which subsequently oxidize in the oxidation layer to H_2O and CO_2. This description of the flame structure considerably simplifies the analysis. It was also found that the structure premixed flames and partially premixed flames consist of these distinct layers. This finding implies that accurate analytical description of the combustion process in laminar flamelets are possible, and the results can be extended to turbulent flames.

TABLE OF CONTENTS

	PAGE
List of Personnel, Publications	1
Abstract	3
I. Chapter I Introduction	4
II. Chapter II Heptane-Air Diffusion Flames	6
II.1 Structure of Heptane-Air Counterflow Diffusion Flames	6
II.2 Comparison Between Experimental Measurements and Numerical Calculations of the Structure of Heptane-Air Diffusion Flames	7
III. Chapter III Analysis of the Structure and Mechanisms of Extinction of Counterflow Methanol-Air Diffusion Flame	41
IV. Chapter IV Asymptotic Structure and Extinction of Methane-Air Diffusion Flames	43
V. Chapter V Methane-Air Premixed Flames	45
V. 1 Comparison Between Experimental Measurements And Numerical Calculations of the Structure of Counterflow, Diluted, Methane-Air, Premixed Flames	45
V. 2 The Inner Structure of Methane-Air Flames	47
V. 3 The Asymptotic Structure of Nonstoichiometric Methane-Air Flames	49
VI. Chapter VI The Structure and Extinction of Partially Premixed Flames Burning Methane in Air	83
VII. Chapter VII. Hydrogen-Air Diffusion Flames	84
VII. 1 Analysis of the Structure of Counterflow Hydrogen-Air Diffusion Flames	84

VII. 2 The Influence of Lewis Number of the Reactants on the Asymptotic Structure of Counterflow and Stagnant Diffusion Flames..... 85

Scientific personnel who participated in the project were:

1. Dr. Kalyanasundaram Seshadri, Associate Professor of Chemical Engineering.

2. Dr. Anthony Peter Hamins.

3. Dr. Chi Ping Lee.

4. Dr. Ishwar Puri.

5. Captain Jesse Crump

6. Ms. Mary Bui-Pham, Candidate for a Ph. D degree in Engineering

7. Mr. David Blackburn, Undergraduate Research Assistant

8. Ms. G. Wilson:

List of publications resulting from this project

1 Hamins, A., Gordon, A. S., Seshadri, K., and Saito, K. : The Structure of Coflowing, Laminar C_2 Hydrocarbon-Air Diffusion Flames, Twenty-first (International) on Combustion, The Combustion Institute, pp 1077-1083, 1986.

2. Smooke, M. D., Seshadri, K., and Puri, I. K.: The Structure and Extinction of Partially Premixed Flames Burning Methane in Air, Twenty-Second Symposium (International) on Combustion, The Combustion Institute, pp 1555-1563, 1988

3) Seshadri, K., and Peters, N.: Asymptotic Structure and Extinction of Methane-Air Diffusion Flames, Combust. Flame 73, pp 23-44, 1988.

4) Seshadri, K., Trevino, C., and Smooke, M. D: Analysis of the Structure and Mechanisms of Extinction of a Counterflow Methanol-Air Diffusion Flame, Combust. Flame, 76, pp 111-132, 1989.

5) Seshadri, K., and Trevino, C.: The Influence of Lewis Number of the Reactants on the Asymptotic Structure of Counterflow and Stagnant Diffusion Flames, Combust. Sci. Tech. 64, pp 243-261, 1989.

6) Bui, M., Seshadri, K., and Williams, F. A.: Structure of Heptane-Air Counterflow Diffusion Flames" Proceedings of the Fourth International Conference on Supercomputing and Third World Supercomputing Exhibition (Eds. L. P. Kartashev, and S. I. Kartashev), April 30 - May 5, 1989, Volume II, pp 490-495.

7) Tangirala, V., Seshadri, K., Trevino, C., and Smooke, M. D.: Analysis of the Structure of Counterflow Hydrogen-Air Diffusion Flames, to appear in Progress in Astronautics and Aeronautics, 1990.

8) Seshadri, K., and Peters, N.: The Inner Structure of Methane-Air Premixed Flames, Combust. Flame 81, pp 96-118, 1990

9) Smooke, M. D., Crumb, J., Seshadri, K., and Giovangigli: Comparison Between Experimental Measurements and Numerical Calculations of the Structure of Counterflow, Diluted, Methane-Air Premixed Flames, to appear in Twenty-Third (Symposium) International on Combustion, The Combustion Institute, 1990

10) Bui-Pham, M., and Seshadri, K.: Comparison Between Experimental Measurements and Numerical Calculations of the Structure of Heptane-Air Diffusion Flames, submitted for publication in Combustion Science and Technology, 1990.

11) Goettgens, J, Peters, N., Seshadri, K., and Williams, F. A.: The Asymptotic Structure of Nonstoichiometric Methane-Air Flames, in preparation 1990

ABSTRACT

The principal objective of this research is to obtain an improved understanding of the structure of laminar flames burning hydrocarbon fuels, alcohol fuels, and blends of hydrocarbon and alcohol fuels. This work attempts to support the U. S. Army's research and development programs in alternative fuels. Since, there is convincing evidence that turbulent reacting flows can be modelled as statistical ensemble of laminar flamelets, an experimental, numerical and analytical study was undertaken to clarify the structure and mechanisms of extinction of laminar diffusion flamelets, laminar premixed flamelets and laminar partially premixed flamelets.

Results of the study on diffusion flames burning hydrocarbon and alcohol fuel show that the basic structure of these flames are essentially similar and can be modelled by use of four overall reactions. Only one of these overall reactions is specific to the fuel being considered, while the other three reactions are those which describe the oxidation of H_2 and CO to H_2O and CO_2. It was found that chemical reactions occur in roughly two distinct layers which are termed the inner layer and the oxidation layer. In the inner layer the fuel is attacked by the radicals to form H_2 and CO, which subsequently oxidize in the oxidation layer to H_2O and CO_2. This description of the flame structure considerably simplifies the analysis. It was also found that the structure premixed flames and partially premixed flames consist of these distinct layers. This finding implies that accurate analytical description of the combustion process in laminar flamelets are possible, and the results can be extended to turbulent flames.

CHAPTER I

INTRODUCTION

The objective of this research was to support the U. S. Army research and development program in alternative fuels. The research was performed in collaboration with Professor N. Peters at the Institut of Technische Mechanik, Rheinish-Westfalische Technische Hochschule at Aachen, West Germany, Professor C. Trevino at Depto Fluidos y Termica, Facultad de Ingenieria, UNAM, Mexico, and Professor M. D. Smooke at the Department of Mechanical Engineering, Yale University, New Haven, Connecticut.

The principal objective of this research is to obtain an improved understanding of the combustion of hydrocarbon and alcohol fuels. Simple, but fundamentally sound methods for evaluating the combustion of hydrocarbon fuels have also been developed. The structure of premixed flames and diffusion flames were considered. In the previous contract entitled "Mechanisms of Combustion of Hydrocarbon/Alcohol Fuel Blends", experiments were performed to characterize the structure of diffusion flames burning hydrocarbon fuels, alcohol fuels and blends of hydrocarbon and alcohol fuels. A major effort in the present program involved interpretation of these experimental results. Detailed numerical calculations and asymptotic analysis was performed to interpret these experimental results. The techniques developed here can be readily extended to most hydrocarbon fuels and fuel blends.

Since most of the results of this research have been published in the open unclassified literature, only the abstract of these published work is given here, and the reader is referred to the literature for further details. Results of research which have been submitted for publication are reproduced here.

In Chapter II results of numerical studies on heptane-air diffusion flames are reported. It was found that the chemical kinetic mechanism for oxidation of heptane can be reduced to four overall reactions. In Chapter III a corresponding numerical study was performed on methanol-air diffusion flames, and the results show that the overall chemical kinetic mechanism of

oxidation of methanol can also be reduced either to five overall reactions. Although these numerical studies provide valuable information concerning the structure of these flames they require substantial computer time. In addition, numerical techniques may mask the underlying physics of the phenomena. Asymptotic analysis on the other hand require minimal computer time, and often clarify the essential physics of the phenomena. In order to develop asymptotic techniques for analyzing the structure of hydrocarbon flames, studies were made on simple hydrocarbon fuels such as methane and the results are summarized in Chapter IV. Since turbulent combustion can be modelled as a statistical ensemble of laminar diffusion flamelets, laminar premixed flamelets, and laminar partially premixed flamelets, experimental, numerical and asymptotic studies were performed on laminar premixed flames and they are reported in Chapter V. Similarly in Chapter VI studies on partially premixed flames are reported. It was found that that hydrogen-oxygen reactions play an in the combustion of hydrocarbon and alcohol fuels. Therefore, a numerical and analytical study was undertaken to determine the structure of hydrogen-air diffusion flames and the results are summarized in Chapter VII. Since, the characteristic Lewis Number of hydrogen is small, differential diffusion of this species plays an important role in determining the structure of the flame. Hence, in Chapter VII, results of analytical studies of the influence of Lewis Number of the reactants on the asymptotic structure of counterflow diffusion flames are also summarized.

CHAPTER II HEPTANE - AIR DIFFUSION FLAMES

II .1 STRUCTURE OF HEPTANE-AIR COUNTERFLOW DIFFUSION FLAMES

The Supercomputer located at the NSF Center at San Diego was used to characterize the structure of heptane-air diffusion flames. The computer program and formulation for the numerical problem used in these calculations were developed by Professor M. D. Smooke at Yale University. The chemical kinetic mechanism for oxidation of heptane used in this paper consists of forty-two elementary reactions involving eighteen species. The balance equations for mass, momentum, energy, and species were integrated numerically, and converged solutions were typically obtained using approximately four hours of CPU time. The results of numerical calculations were compared with experimental measurements, and good agreement was obtained.

The research summarized above has been published in the Proceedings of the Fourth International Conference on Supercomputer and Third World Supercomputer Exhibition, Volume II, Edited by Professor Lana P. Kartashev and Dr. Steven I. Kartashev, International Supercomputing Institute, Inc, Suite B-309, 3000-34th Street, South. St. Petersburgh, Florida 33711, pp 490-495, 1989. The coauthors of this publication were Ms. Mary Bui-Pham and Professor F. A. Williams

II. 2 COMPARISON BETWEEN EXPERIMENTAL MEASUREMENTS AND NUMERICAL CALCULATIONS OF THE STRUCTURE OF HEPTANE-AIR DIFFUSION FLAMES

ABSTRACT

Detailed numerical calculations are performed to determine the structure of heptane-air diffusion flames, and the results are compared with experimental measurements. The configuration used is the diffusion flame stabilized in the vicinity of a stagnation plane, which is formed by directing an oxidizing gas flow onto the vaporizing surface of a pool of heptane. Profiles of the concentration of various stable species and of the temperature have been measured by gas chromatography and by thermocouples, respectively. To evaluate the influence of strain on the structure of the flame, the measurements taken at a fixed composition of the oxidizer stream and at two values of the strain rate were chosen for comparison with the calculated results. The computations were performed using a chemical kinetic mechanism consisting of forty-two elementary reactions involving eighteen species. To simplify the chemical kinetic mechanism, it was assumed that heptane is attacked by radicals to form the heptyl radical whose decomposition to CH_3 and C_3H_6 is represented by a one-step overall reaction. Good agreement was obtained between the results of the detailed numerical calculations and the experimental measurements. It was found that aspects of the structure of heptane-air diffusion flames relevant to asymptotic descriptions are similar to those of methane-air diffusion flames. Hence, the previously developed techniques for asymptotic analysis of the structure of methane-air flames can be used for analyzing the structure of heptane-air flames.

1. INTRODUCTION

Motivated by recent success in numerical and analytical modeling of the structure of laminar flames burning simple hydrocarbon fuels such as methane and propane, Warnatz (1984), Esser et al. (1985), and Westbrook et al. (1988) have studied the combustion of more complex hydrocarbon fuels such as n-heptane and iso-octane which are often used as reference fuels. These previous investigations have been concerned with premixed systems. In this paper, results of numerical calculations of heptane-air diffusion flames structure are reported and compared with previous experimental measurements made by Kent and Williams (1974), Seshadri (1977), and Hamins and Seshadri (1987). The calculations were performed on the Cray X-MP located at the NSF Center at San Diego using a program developed by Smooke (1982).

To use a nearly complete description of the chemical kinetics of oxidation of heptane in the calculations would be difficult because it involves hundreds of elementary reactions containing numerous species, some of which would have several isomeric structures. For example, Warnatz (1984) suggested that there may exist 39 isomeric structures for the principal alkyl radical which is formed from heptane. Since the structures of steady diffusion flames are of interest here, only the high temperature oxidation of heptane is relevant. Warnatz (1984) has also outlined a procedure for characterizing the chemical kinetic mechanism of oxidation of higher alkanes including heptane. It is presumed that alkanes are attacked by the radicals H, O, and OH to form the alkyl radical which decomposes to smaller radicals by fast thermal elimination of alkenes to eventually form CH_3 and C_3H_6; reactions leading to these compounds are not presumed to be rate limiting. This approximation considerably simplifies the chemistry because the oxidation of CH_3 and C_3H_6 is better understood. Using this approximation, Warnatz (1984) calculated the burning velocities of premixed flames for a number of higher hydrocarbon fuels including

heptane and found good agreement between the calculated values and experimental measurements. The calculated burning velocities were found to be relatively insensitive to variations, within reasonable limits, of the rate of decomposition of the principal alkyl radical to CH_3 and C_3H_6. Therefore, in these calculations, the decomposition of C_7H_{15} was represented by a one-step reaction to form CH_3 and C_3H_6, and the rate of this reaction was chosen to be equal to that of decomposition of the n-butyl radical. Studies of this type are useful in identifying key reactions characterizing the structure and mechanisms of oxidation of hydrocarbon fuels. The results obtained here are useful for future asymptotic analyses using multi-step overall chemical kinetic models similar to those performed by Seshadri and Peters (1988) for methane-air diffusion flames.

2. DESCRIPTION OF THE EXPERIMENTAL MEASUREMENTS AND FORMULATION OF THE NUMERICAL PROBLEM

2.1 Description of the Experimental Measurements:

Experiments were performed by Kent and Williams (1974), Seshadri (1977), and Hamins and Seshadri (1987) to determine the structure of diffusion flames stabilized in the stagnation point boundary layer by directing an oxidizing gas stream vertically downward onto the vaporizing surface of pools of heptane. The oxidizer duct was located 1 cm above the fuel surface; a diffusion flame can be indefinitely stabilized in this configuration. Seshadri and Williams (1978) suggested that the strain experienced by the flame sheet can be approximated if the flow velocity at the exit of the oxidizer duct is known, and for given values of strain and composition of the oxidizing gas, the fuel burning rate and the surface temperature can be calculated if the thermodynamics of vaporization and oxidation are known.

Concentration profiles of stable species were measured using gas chromatographic techniques, and temperature profiles were measured by thermocouples. The two sets of experimental measurements chosen for comparison with numerical calculations are: 1) $Y_{O_2\infty}$ = 0.185, U= 30.5 cm/s, and 2) $Y_{O_2\infty}$ = 0.185, U= 83.7 cm/s, where $Y_{O_2\infty}$ and U are the mass fraction and axial velocity of the oxidizing gas stream at the exit of the duct, respectively. Flames at two different values of strain with the same values of $Y_{O_2\infty}$ are considered here to clarify the influence of strain on the structure of the flame. Since the theoretically calculated strain rate is directly proportional to the velocity of the oxidizing gas at the exit of the duct, the increase in the strain rate can be obtained by increasing the oxidizer stream velocity. Experimental data for U = 30.5 cm/s were collected by Kent and Williams (1974), and those for U= 83.7 cm/s are shown in Figs. 8 and 9. Further details of the experimental apparatus and procedure for making these measurements are outlined by Kent and Williams (1974), Seshadri (1977), and Hamins and Seshadri (1987).

2.2 Chemical Kinetic Mechanism:

Table 1 shows the chemical kinetic mechanism used in the calculations. The rate constants are assumed to be in the Arrhenius form, $k_j = A_j T^{nj} \exp(-E_j / (RT))$, where A_j is the frequency factor, n_j is the temperature exponent, and E_j is the activation energy. The data shown in Table 1 represent the forward rate of the reactions; the backward rates are calculated from the equilibrium constant.

The data selected for the rate constants for reactions 1-33 were obtained from published work of Warnatz (1984), Westbrook and Dryer (1984), and Miller et al (1984), and they are similar to those used previously by Smooke et al. (1986), Puri et al. (1987), and Smooke et al. (1988) for methane-air flames and partially premixed flames. The results of the numerical calculations using these rates were found to agree well with

experimental measurements. The data selected for the rates of reactions 34-96 are those recommended by Warnatz (1984).

2.3 Formulation of the Numerical Problem:

The formulation of the numerical problem is described in detail by Smooke et al. (1986); hence, only the main features are outlined here. Let r and z denote the independent spatial coordinates in the radial and axial directions, respectively. The primary oxidizer stream is located at $z = L_\infty$, and the surface of the liquid fuel at $z = 0$. The experimental flow-field consists of an inner, viscous flow region near the fuel surface which extends slightly beyond the stagnation plane into the oxidizer side and an outer, inviscid, and rotational region extending from the oxidizer side of the stagnation plane to the exit of the oxidizer duct, where the tangential component of the flow velocity vanishes. Hence, in the outer flow, the strain rate a is a function of the axial coordinate z, as suggested by Seshadri and Williams (1978). However, in the computational model used here, the outer flow is assumed to be inviscid and irrotational, and the tangential component of the flow velocity u_∞ at the oxidizer duct is not zero. Thus, in the outer flow, the value of a is constant, and the tangential and normal component, u and v, at the edge of the boundary layer can be written as $u_\infty = ar$, and $v_\infty = -2az$, where ∞ denotes conditions at the primary oxidizer stream at $z = L_\infty$. Hence, the computational model used for the outer flow is different than that encountered in the experiment and results in a slight shift in the flame location. A more accurate description of the flow field incorporating the rotational aspect of the outer flow is described by Kee et al. (1988).

The notations $f' = u/u_\infty$ and $M = \rho v$ are introduced, where f' is related to the derivative of a modified stream function, as suggested by Dixon-Lewis et al. (1984), and ρ

is the gas density. The governing boundary layer equations for mass, momentum, chemical species and energy in cylindrical coordinates are:

$$\frac{dM}{dz} + 2a\rho f' = 0$$

$$\frac{d}{dz}\left(\mu \frac{df'}{dz}\right) - M \frac{df'}{dz} + a\left(\rho_\infty - \rho (f')^2\right) = 0$$

$$-\frac{d}{dz}\left(\rho Y_k V_k\right) - M \frac{dY_k}{dz} + \dot{w}_k W_k = 0, \quad k = 1, 2, ..., K$$

$$\frac{d}{dz}\left(\lambda \frac{dT}{dz}\right) - c_p M \frac{dT}{dz} - \sum_{k=1}^{K} \rho Y_k V_k c_{pk} \frac{dT}{dz} - \sum_{k=1}^{K} \dot{w}_k W_k h_k = 0$$

and the system is closed with the ideal gas law

$$\rho = p\overline{W} / (RT)$$

In the above set of equations, T denotes the temperature; Y_k, the mass fraction of the k^{th} species; p, the pressure; $\dot{w}_k$, the molar rate of production of the k^{th} species; W_k, the molecular weight of the k^{th} species; $\overline{W}$, the mean molecular weight of the mixture; R, the universal gas constant; λ, the thermal conductivity of the mixture; c_p, the heat capacity of the mixture; c_{pk}, the heat capacity of the k^{th} species; h_k, the specific enthalpy of the k^{th} species; μ, the viscosity of the mixture, and V_k is the diffusion velocity of the k^{th} species in the z direction. Equations for determining V_k, and $\dot{w}_k$ are outlined by Kee et al. (1983). Since the mass flux and composition of the oxidizing gas at the exit of the duct are known, the undetermined strain rate can be calculated as an eigenvalue of the problem by introducing the differential equation da/dz = 0.

To complete the specifications of the problem, appropriate boundary conditions must be imposed. At the oxidizer jet located at $z = L_\infty$, the conditions consistent with the model used for the outer flow are:

$$f' = 1 \; ; \; Y_{O_2} = Y_{O_2\infty}, \; Y_k = 0, \; k \neq O_2, N_2 \; ; \; M = M_\infty \; ; \; T = T_\infty$$

At the surface of the liquid fuel, the tangential component of the flow velocity is presumed to be zero (no slip), and the appropriate interface balance conditions are:

$$f'_w = 0$$
$$\rho_w Y_{kw} V_{kw} + M_w Y_{kw} = 0, \; k = 1, 2, \ldots, K; \; k \neq F$$
$$\rho_w Y_{Fw} V_{Fw} + M_w Y_{Fw} = \dot{m} = M_w$$
$$\left[\lambda \frac{dT}{dz}\right]_w = M_w L$$

Here $\dot{m}$ is the unknown mass burning rate and will be determined as part of the solution; L is the latent heat of vaporization of the fuel ; F refers to the fuel, and w refers to conditions on the gas side of the liquid gas interface. To determine the surface temperature of the fuel, it is presumed that there exists gas-vapor equilibrium at the interface, which is an excellent approximation for the values of $\dot{m}$ encountered here.

The governing equations form a system of nonlinear two-point boundary value problems. The solution procedure as developed by Smooke (1985) employs a flame sheet starting model with an adaptive time-integration and finite difference method. Initially, the surface temperature of the fuel T_W was assumed to be equal to the normal boiling point, and a converged solution was obtained assuming a reasonable value for the burning rate $\dot{m}$ using the boundary conditions at the oxidizer duct exit and all of the liquid-gas interface balance equations, except that for energy balance. To calculate T_W for vapor-liquid

equilibrium at the interface, the computed value of the concentration of the fuel in the gaseous form Y_{FW} and the thermodynamic data collected by Rossini et al. (1947) were used. A revised value for $\dot{m}$ was calculated using the energy balance condition, the computed values of the temperature gradient $(dT/dz)_W$, and λ on the gas side of the interface. Calculations were repeated using these revised values of T_W and $\dot{m}$ until the changes in their values were less than 2%.

3. RESULTS AND DISCUSSION

3.1 Simplification of the Chemical Kinetic Mechanism:

To simplify the chemical kinetic mechanism, the numerical calculations were initially performed to determine the structure of diffusion flames stabilized near the stagnation region formed between two steady, laminar, infinitely wide, axisymmetric counterflowing jets of heptane vapor diluted with nitrogen and air. The calculations were performed using the chemical kinetic mechanism and rate data shown in Table 1 and for a value of the strain rate, a, equal to 9.84 s^{-1}. Results of the computations are interpreted using a suitably defined mixture fraction, Z, as the independent variable. This permits analysis to be performed without reference to specific flow configurations. There exist several definitions of the mixture fraction, that introduced by Peters (1984) which is based on the elements present in the fuel, that introduced by Bilger (1984) which is based on the elements carbon and hydrogen present in the fuel and oxygen in the oxidizer stream, and that introduced by Tangirala et al. (1989) which is based on an inert species in the system such as nitrogen. Although the definition introduced by Bilger (1984) is employed here, the qualitative and quantitative results obtained using other definitions were essentially the same for heptane-air flames. The mixture fraction Z can be expressed by the relation

exactly equal to zero at the injection plane; thus, the value of a can be expected to lie between 24.8 and 30.5 s^{-1}, although probably closer to the latter value. Hence, the slight shift between the computed and measured peak temperature may be at least partially attributed to inaccuracies in the flow field descriptic Experimental uncertainty in probe positioning may also play a role.

Asymptotic analysis of the structure of diffusion flames, as discussed by Williams (1985) and Rossini (1947), shows that the outer flow affects the flame location, and the chemistry is confined to the inner zone where there exists a diffusive-reactive balance. Hence, if the results are plotted using the defined mixture fraction Z as the independent variable, then better agreement can be expected.

In Fig. 7, the results shown in Fig. 6 are replotted versus Z and show that the measured and calculated peak flame temperature occur at nearly the same value of $Z \approx 0.055$. Similarly, the measured and calculated profiles of C_7H_{16}, O_2, and H_2 are aligned and show good agreement. However, the computed values of CO_2, H_2O, and CO are higher than the corresponding measured values, as is also seen in Fig. 6. Since the reaction rates along the path where H_2 and CO are oxidized to H_2O and CO_2 are reasonably well understood, a potential source of the discrepancies could be inaccuracies in the reaction rates along the paths, shown in Fig. 4, where C_7H_{16} is converted to CH_3; a lower rate along the latter path could provide better agreement. When the reaction rates along this path were examined, we found that the rate of reaction 37, $C_3H_6 + O \rightarrow 2\ CH_3 + CO$, is slowest among the fastest rates. Therefore, calculations were made using a frequency factor for reaction 37 which is 10 times lower than that originally used. However, no significant changes in peak concentration for the stable species were detected, which indicates that the rates for these early steps are not responsible for the discrepancies. As a further exploratory check, numerical calculations were repeated with the frequency factor of

$$Z = \frac{(22/7)\, Y_C / W_C + (22/16)\, Y_H / W_H + (Y_{O,O} - Y_O) / W_O}{(22/7)\, Y_{C,F} / W_C + (22/16)\, Y_{H,F} / W_H + Y_{O,O} / W_O}$$

where $$Y_m = \sum_{i=1}^{K} a_{im}\, W_m\, Y_i / W_i$$

here a_{im} is the stoichiometric coefficient denoting the number of atoms of element m in a molecule of species i; $Y_{m,F}$ is the value of Y_m in the fuel, and $Y_{O,O}$ is the value of Y_O in the ambient oxidizer stream.

The dashed lines in Figs. 1 and 2 show profiles of temperature and concentration of the major stable species (C_7H_{16}, O_2, CO_2, H_2O, H_2 and CO) calculated using all the 96 elementary chemical reactions shown in Table 1. The dashed lines in Fig. 3 show similar profiles for selected radicals (H, OH, O and HO_2). The profiles of the reaction rates of the various elementary reactions were also calculated. The results of these calculations were used to deduce the principal path of oxidation of heptane which is shown schematically in Fig. 4. The fuel is attacked by the radicals H, OH, and O to form C_7H_{15} which decomposes to form CH_3 and C_3H_6. Propene is then attacked by radicals to form CH_3 and CH_3HCO, and CH_3HCO reacts with radicals to form additional CH_3. Subsequent oxidation proceeds similarly to that in methane-air diffusion flames. CH_3 reacts with radicals to form formaldehyde which produces HCO followed by the formation of H_2 and CO, which are oxidized to form H_2O and CO_2.

To simplify the chemical kinetic mechanism, all species which are not formed or destroyed along the principal path of oxidation of heptane shown in Fig. 4 were removed. Consequently, reactions 43-96 which involve the species CH_4, CH_2, CH, C_2H, C_2H_6, C_2H_5, C_2H_4, C_2H_3, C_2H_2, C_3H_8, C_3H_7, CH_2CO, and C_2HO were eliminated. The solid

lines in Figs. 1, 2, and 3 represent profiles calculated using reaction 1-42 shown in Table 1, and they agree reasonably well with the profiles calculated using the complete set of reactions 1-96. Hence, further calculations were performed using reactions 1-42.

3.2 Comparison between Numerical Calculations and Experimental Measurements:

Numerical calculations were performed on a domain of 1.00 cm. For the cases of U = 30.5 cm/s and U = 83.7 cm/s, the mass fluxes at the exit of the duct, M_∞, were 0.0358 gm/cm^2/s and 0.098 gm/cm^2/s, respectively, and the temperature of the ambient oxidizing gas stream was T_∞ = 298 K.

Fig. 5 shows the calculated profiles of the axial velocity along the axis of symmetry. In both cases, the stagnation plane lies close to the fuel surface and moves closer with increasing strain. In Fig. 6, experimentally measured profiles (shown as points) for temperature and the stable species C_7H_{16}, O_2, CO_2, H_2O, H_2, and CO are compared with the calculated values (shown as lines) for U = 30.5 cm/s, and the shapes show good agreement. However, the computed peak temperature occurs 0.4 mm nearer the oxidizer side than the measured peak temperature; a similar shift is also observed for the species profiles. A similar but larger effect was found previously for methane-air diffusion flames by Smooke et al. (1986) and Puri et al. (1987) and is partially attributed, as mentioned in section 2.3, to the difference between the experimental and computational flow field. The calculated strain rate was 24.68 s^{-1}. However, Seshadri and Williams (1978) showed that, if the outer flow is assumed to be inviscid and rotational, then a = U/L = 30.5 s^{-1} at the stagnation plane which is presumed to coincide with the surface of the fuel. If the calculations are repeated with this higher value of a, then the peak temperature decreases by 15 K and occurs 0.275 mm nearer the fuel side than the measured peak temperature. However, the tangential component of the oxidizer velocity in the experiments may not be

the rate of reaction 25, HCO + M --> H + CO + M, lowered to 1.6 x 10^{13}, and the calculated peak concentration of CO shows better agreement; however, the discrepancies for CO_2, H_2O still remain. Hence, it appears that the discrepancies can be attributed mainly to experimental inaccuracies, especially since the differences are comparable in magnitude with estimated experimental uncertainties.

Peters (1984) showed from an asymptotic analysis of the outer zone that if the chemical reaction was presumed to occur as a one-step irreversible process, C_7H_{16} + 11 O_2 --> 7 CO_2 + 8 H_2O, and if the Lewis number of all species are presumed to be nearly unity, then the value of Z, at the position where carbon, hydrogen, and oxygen are in stoichiometric proportions, is Z_{st} = 0.05 where maximum flame temperature occurs. Recently, Seshadri and Peters (1988) performed an asymptotic analysis of the structure of methane-air diffusion flames using realistic flame chemistry to show that the peak temperature occurs at a value of Z which is larger than Z_{st}, and our computations support this result for heptane-air diffusion flames.

In Figs. 8 and 9, the experimental profiles for temperature and the stable species C_7H_{16}, O_2, CO_2, H_2O, H_2, and CO are compared with those calculated for U = 83.7 cm/s using the physical variable z and the mixture fraction Z as the independent variable, respectively. The agreement between the experimental and calculated values is not as good, which is expected because of greater experimental difficulties in spatial resolution at this higher strain rate. However, the agreement is qualitatively similar to that shown in Figs. 6 and 7. Fig. 10 shows the calculated profiles for the radicals H, OH, O, and HO_2 for U = 30.5 cm/s and U = 83.7 cm/s and is discussed below.

3.2 Influence of Strain Rate:

To evaluate the influence of strain on the structure of heptane-air flames, some interesting features of Figs. 5-10 are shown in Table 2. With increasing flow velocity of the oxidizer stream (increasing strain), the stagnation plane moves toward the fuel surface, and the flame standoff distance, which is defined as the distance between the peak value of the flame temperature and the fuel surface, decreases. Also with increasing strain, the fuel burning rate increases because the higher molar flow rate of oxidizer must be matched with that of the fuel, such that at the flame, the flow rate of the reactants are in stoichiometric proportions. Table 2 shows that, with increasing strain, the maximum flame temperature decreases, and the oxygen concentration at that position increases. Hence, leakage of oxidizer through the reaction zone increases with strain. However, the leakage of the fuel, which is represented by the fuel concentration at maximum temperature, is negligibly small in both cases.

These results are consistent with those of asymptotic analysis done by Linan (1974), Miller et al. (1984), Tangirala et al. (1989), Seshadri and Peters (1988), which show that with increasing strain, the flame temperature must decrease, and the leakage of the reactants through the flame must increase. However, Linan (1974) showed that, when the chemistry for the hydrocarbon flames is approximated by a one-step, irreversible reaction, the leakage of fuel through the reaction zone is considerably higher than that of oxygen with increasing strain. Whereas results using realistic chemistry, as reported by Seshadri and Peters (1988), show that the leakage of oxygen through the reaction zone increases with increasing strain, and the leakage of fuel is negligible. Hence, the numerical results are qualitatively consistent with asymptotic analysis results using realistic chemistry.

Table 2 shows that the value of Z at the surface of the liquid pool increases with increasing strain, and this is due to the increasing fuel concentration at the liquid pool surface. Table 2 also shows considerable discrepancy between the measured and computed oxygen concentration at maximum temperature; this is probably due to inaccuracies associated with measuring small oxygen concentrations using a gas chromatograph since the uncertainties in the numerical results are considerably smaller. This conclusion was also reached in previous comparisons of experimental measurements and numerical calculations for methane-air flames done by Smooke et al. (1986) and Puri et al. (1987). Fig. 10 shows that, although the peak concentration of the radicals H, OH, and O do not change much with increasing strain, the peak concentration of HO_2 increases sharply, and this is consistent with the steady-state approximation for HO_2, as reported by Seshadri and Peters (1988).

3.3 Prospect for Asymptotic Description:

It is useful to compare certain aspects of the structure of heptane-air diffusion flames relevant for asymptotic description with similar ones of methane-air diffusion flames. If as assumed previously for methane-air diffusion flames, the concentration of all species except those for C_7H_{16}, O_2, CO, H_2, H, H_2O, CO_2, and N_2 are presumed to be in a dynamic steady state, then using the procedures outlined by Peters (1985), it can be shown that the chemical kinetic mechanism for heptane oxidation can be simplified to the following four overall reactions:

$$C_7H_{16} + 10\,H + 7\,H_2O \text{ ---> } 7\,CO + 20\,H_2 \qquad (1)$$

$$CO + H_2O \text{ <===> } CO_2 + H_2 \qquad (2)$$

$$H + H + M \text{ ---> } H_2 + M \qquad (3)$$

$$O_2 + 3\,H_2 \text{ <===> } 2\,H + 2H_2O \qquad (4)$$

The rates of these four overall reactions can be related to the rates of elementary reactions shown in Table 1. In Fig. 8, the computed profiles for the species appearing in the above overall reactions are shown for U = 30.5 cm/s. Two separate regions are identified and labeled as the "fuel consumption layer" and the "oxygen consumption layer". In the fuel-consumption layer, radicals such as H atoms attack the fuel to form CO and H_2 in accord with the overall reaction 1. Because of the strong affinity of the fuel to the radicals, further oxidation of the intermediate species H_2 and CO is inhibited in this layer; consequently, the concentrations of H_2 and CO attain a maximum value in the fuel consumption layer. After the fuel is nearly consumed on the oxidizer side of the flame, there exists an "oxygen-consumption layer", where the overall reactions 3-4 occur, and radicals are produced to react with H_2 and CO to form the final products H_2O and CO_2. Thus, the calculations clearly show that certain aspects of the structure of heptane-air diffusion flame relevant for asymptotic description are similar to those of methane-air diffusion flames, as shown by Peters (1985). This offers considerable simplification because it implies that the techniques developed for analyzing the structure of methane-air flames can be extended to heptane-air flames.

4. CONCLUSION

Detailed numerical calculations were performed to determine the structure of heptane-air diffusion flames, and the results were compared with experimental measurements. The following remarks summarize the major conclusions:

1. The calculated profiles of temperature and stable species were found to agree well with the experimental measurements, but the computed peak temperature was shifted slightly and was attributed to the inaccurate description of the flow field. However,

better alignment was obtained when the profiles were plotted using the mixture fraction as the independent variable.

2. With increasing strain, the burning rate increases, the peak temperature decreases, and the oxygen leakage increases.

3. Key aspects of the structure of heptane-air diffusion flames are similar to those of methane-air diffusion flames; hence, previously developed techniques for asymptotic analysis can be extended to heptane-air flames.

The research summarized above has been submitted for publication in Combustion Science and Technology. The coauthor of the publication is Ms. Mary Bui-Pham.

ACKNOWLEDGEMENTS

The authors acknowledge the invaluable assistance of Professor M. D. Smooke at Yale University for providing the computer program which was used to perform the numerical calculations reported here and for continued advice in trouble-shooting. The authors also acknowledge stimulating discussions with Professor F. A. Williams and Dr. Venkat Tangirala, concerning various aspects of this work. This research was supported by the U. S. Army Research Office Contract # DAAL 03-8G-K 0001. Dr. David Mann is the Technical Monitor of the program.

REFERENCES

Dixon-Lewis, G., David, T., Gaskell, P. H., Fukutani, S., Jinno, H., Miller, J. A., Kee, R. J., Smooke, M. D., Peters, N., Effelsberg, E., Warnatz, J., and Behrendt, F. (1984). Calculation of the structure and extinction limit of a methane-air counterflow diffusion flame in the forward stagnation region of a porous cylinder. *Twentieth Symposium (International) on Combustion*, The Combustion Institute, Pittsburgh, p. 1893.

Esser, C., Maas, U., and Warnatz, J.(1985). *International Symposium on Diagnostics and Modelling of Combustion in Reciprocating Engines, JSME, SAEJ, MESJ*, Tokyo, p. 355.

Hamins, A., and Seshadri, K. (1987). The Structure of diffusion flames burning pure, binary and ternary solutions of methanol, heptane, and toluene. *Combustion and. Flame* **68**, p. 295.

Kee, R. J., Warnatz, J., and Miller, J. A. (1983). A Fortran computer package for the evaluation of gas-phase viscosities, conductivities, and diffusion coefficients. Sandia National Laboratories Report SAND 83-8209.

Kee, R. J., Miller, J. A., Evans, G. H., and Dixon-Lewis, G. (1988). A computational model of the structure and extinction of strained, opposed flow, premixed methane-air flames. *Twenty-Second Symposium (International) on Combustion*, The Combustion Institute, Pittsburgh, p. 1479.

Kent, J. H., and Williams, F. A. (1974). Extinction of laminar diffusion flames for liquid fuels. *Fifteenth Symposium (International) on Combustion*, The Combustion Institute, Pittsburgh, p. 315.

Krishnamurthy, L., Williams, F. A., and Seshadri, K. (1976). Asymptotic theory of diffusion-flame extinction in a stagnation-point boundary layer *Combustion and Flame* **26**, p. 363.

Linan, A. (1974). The asymptotic structure of counterflow diffusion flames for large activation energies. *Acta Astronautica* **1**, p.1007.

Miller, J. A., Kee, R. J., Smooke, M. D., and Grcar, J. F. (1984). The computation of the structure and extinction limit of a methane-air stagnation point diffusion flame. Paper #Wss/Cl 84-10, 1988 Spring Meeting, Western States Section of the Combustion Institute, April 2-3, 1984.

Peters, N. (1985). Invited paper presented at the Symposium of Numerical Simulation of Combustion Phenomena, Sophia-Antipolis (France). Also in *Lecture Notes in Physics* **241** (Eds. R. Glowinski, B. Larrouturou, and R. Teman), Springer Verlag, p. 90.

Peters, N. (1984). Laminar diffusion flamelet models in non-premixed turbulent combustion. *Progress in Energy and Combustion Science* **10**, p. 319.

Puri, I. K., Seshadri, K., Smooke, M. D., and Keyes, D. E. (1987). A comparison between numerical calculations and experimental measurements of the structure of a counterflow methane-air diffusion flame. *Combustion Science and Technology* **56**, p. 1.

Rossini, F. D., Pitzer, K. S., Taylor, W. J., Ebert, J. P., Kilpatrick, J. E., Beckett, C. W., Williams, M. G., and Werner, H. G. (1947). *Selected Values of Properties of Hydrocarbons*, United States Government Printing Office, Washington, D.C.

Seshadri, K. (1977). Studies on flame extinction. Ph. D. Thesis, University of California San Diego.

Seshadri, K., and Williams, F. A. (1978). Laminar flow between parallel plates with injection of a reactant at high Reynolds number *Int. J. Heat and Mass Transfer* **21**, p. 251.

Seshadri, K., and Peters, N. (1988). Asymptotic structure of stoichiometric methane-air flames. *Combustion and Flame* **73**, p. 23.

Smooke, M. D. (1982). Solution of burner-stabilized premixed laminar flames by boundary value methods. *J. Comp. Phys.* **48**, p. 72.

Smooke, M. D. (1983). Error estimate for the modified Newton method with applications to the solution of nonlinear two-point boundary value problems. *J. Opt. Theory and Appl.* **39**, p. 489.

Smooke, M. D., Miller, J. A., and Kee, R. J. (1983). Determination of adiabatic flame speeds by boundary value methods. *Combustion Science and Technology* **34**, p. 79.

Smooke, M. D., Miller, J. A., and Kee, R. J. (1985). *Numerical Boundary Value ODE's*, U. M. Ascher and R. D. Russell (Ed.), Birkhauser, Basel.

Smooke, M. D., Puri, I. K., and Seshadri, K. (1986). A comparison between numerical calculations and experimental measurements of the structure of a counterflow diffusion flame burning diluted methane in diluted air. *Twenty-First Symposium (International) on Combustion*, The Combustion Institute, Pittsburgh, p. 1783.

Smooke, m.D., Puri, I. K., and Seshadri, K. (1988). The structure and extinction of partially premixed flames burning methane in air. *Twenty-Second Symposium (International) on Combustion*, The Combustion Institute, Pittsburgh, p. 1555.

Tangirala, V., Seshadri, K., Trevino, C., and Smooke, M. D. (1989). Analysis of the structure of counterflow hydrogen-air diffusion flames. Paper Presented at the 12th ICDERS Meeting.

Warnatz, J. (1984). Chemistry of high temperature combustion of alkanes up to octane. *Twentieth Symposium (International) on Combustion*, The Combustion Institute, Pittsburgh, p. 845.

Warnatz, J. (1984). *Combustion Chemistry* (Edt. W. C. Gardiner, Jr), p.197.

Westbrook, C. K., and Dryer, F. L. (1984). Chemical kinetic modeling of hydrocarbon combustion. *Prog. Energy Combust. Sci.* **34**, p. 1.

Westbrook, C. K., Warnatz, J., and Pitz, W. J. (1988). A detailed chemical kinetic reaction mechanism for the oxidation of iso-octane and n-heptane over an extended temperature range and its application to analysis of engine knock. *Twenty-Second Symposium (International) on Combustion*, The Combustion Institute, Pittsburgh, p. 893.

Williams, F. A. (1985). *Combustion Theory*, Second Edition, The Benjamin /Cummings Publishing Company, Inc., Menlo Park, California.

LIST OF TABLES AND FIGURES

List of Tables:

1. Chemical kinetic mechanism for oxidation of heptane. Rate coefficients are to be expressed in the form $k_j = A_j T^{n_j} \exp(-E_j/(RT))$. Units are moles, cubic centimeters, seconds, Kelvins and calories/mole.

2. Certain aspects illustrating the influence of strain on structure of heptane-air diffusion flames.

List of Figures:

1. Comparison between the temperature profile calculated using reactions 1-96 (dashed line) with that calculated using reactions 1-42 (solid line) for a = 9.84 s^{-1}.

2. Comparison between concentration profiles for C_7H_{16}, O_2, CO_2 , H_2, CO, and H_2O calculated using reactions 1-96 (dashed lines) with those calculated using reactions 1-42 (solid lines) for a = 9.84 s^{-1}.

3 Comparison between concentration profiles for H, O, OH and HO_2 calculated using reactions 1-96 (dashed lines) with those calculated using reactions 1-42 (solid lines) for a = 9.84 s^{-1}.

4. Schematic illustration of the principal path of oxidation of heptane.

5. Calculated profile of the axial component of the velocity for $Y_{O_{2\infty}} = 0.185$, U = 30.5 cm/s, and U = 83.7 cm/s.

6. Comparison between experimental measurements (shown as points) and computed values (lines) for profiles of temperature and stable species: C_7H_{16}, O_2, CO_2, H_2O, H_2, and CO for $Y_{O_{2\infty}} = 0.185$ and U = 30.5 cm/s

7. Comparison between experimental measurements (shown as points) and computed values (lines) for profiles of temperature and stable species: C_7H_{16}, O_2, CO_2, H_2O, H_2 and CO, using the mixture fraction Z as the independent variable, for $Y_{O_{2\infty}} = 0.185$ and U = 30.5 cm/s.

8. Comparison between experimental measurements (shown as points) and computed values (lines) for profiles of temperature and stable species: C_7H_{16}, O_2, CO_2, H_2O, H_2, and CO for $Y_{O_{2\infty}} = 0.185$ and U = 83.7 cm/s

9. Comparison between experimental measurements (shown as points) and computed values (lines) for temperature and stable species C_7H_{16}, O_2, CO_2, H_2O, H_2, and CO using the mixture fraction Z as the independent variable for $Y_{O_{2\infty}} = 0.185$ and U = 83.7 cm/s.

10. Calculated profiles for the radical H, OH, O, and HO_2 for $Y_{O_2\infty} = 0.185$, U = 30.5 cm/s, and U = 83.7 cm/s.

11. Aspects of the structure of heptane-air diffusion flames relevant for asymptotic description.

TABLE 1

CHEMICAL KINETIC MECHANISM FOR HEPTANE OXIDATION

	Reactions	A	n_j	E
1.	H+O2=OH+O	2.20e+14	0.	16800
2.	H2+O=OH+H	1.80e+10	1.00	8826
3.	OH+H2=H2O+H	1.17e+09	1.30	3626
4.	OH+OH=H2O+O	6.00e+08	1.30	0
5.	H2+M=H+H+M	2.23e+12	0.50	92600
6.	H+OH+M=H2O+M	7.50e+23	-2.60	0
7.	H+O2+M=HO2+M	2.10e+18	-1.00	0
8.	H+O2+N2=HO2+N2	6.70e+19	-1.42	0
9.	H+HO2=OH+OH	2.50e+14	0.	1900
10.	H+HO2=H2+O2	2.50e+13	0.	700
11.	O+HO2=OH+O2	4.80e+13	0.	1000
12.	OH+HO2=H2O+O2	5.00e+13	0.	1000
13.	H2+O2=OH+OH	1.70e+13	0.	47780
14.	H+O2+O2=HO2+O2	6.70e+19	-1.42	0
15.	CO+OH=CO2+H	1.51e+07	1.30	-758
16.	CH3+O=CH2O+H	6.80e+13	0.	0
17.	CH2O+H=HCO+H2	3.31e+14	0.	10500
18.	CH2O+M=HCO+H+M	3.31e+16	0.	81000
19.	CH2O+O=HCO+OH	1.81e+13	0.	3082
20.	OH+CH2O=HCO+H2O	7.53e+12	0.	167
21.	H+HCO=CO+H2	4.00e+13	0.	0
22.	HCO+O=CO+OH	1.00e+12	0.	0
23.	OH+HCO=CO+H2O	5.00e+12	0.	0
24.	O2+HCO=CO+HO2	3.00e+12	0.	0
25.	HCO+M=CO+H+M	1.60e+14	0.	14700
26.	CH3+O2=CH3O+O	7.00e+12	0.	25652
27.	CH3+OH=CH2O+H2	7.50e+12	0.	0
28.	CH3O+M=CH2O+H+M	2.40e+13	0.	28812
29.	CH3O+H=CH2O+H2	2.00e+13	0.	0
30.	CH3O+OH=CH2O+H2O	1.00e+13	0.	0
31.	CH3O+O=CH2O+OH	1.00e+13	0.	0
32.	CH3O+O2=CH2O+HO2	6.30e+10	0.	2600
33.	CH3+O2=CH2O+OH	5.20e+13	0.	34574
34.	CH3HCO+H=CH3+CO+H2	4.00e+13	0.	4200
35.	CH3HCO+O=CH3+CO+OH	5.00e+12	0.	1900
36.	CH3HCO+OH=CH3+CO+H2O	1.00e+13	0.	0
37.	C3H6+O=CH3+CH3+CO	5.00e+12	0.	454
38.	C3H6+OH=CH3HCO+CH3	1.00e+13	0.	0
39.	C7H16+H=C7H15+H2	6.10e+14	0.	8469
40.	C7H16+O=C7H15+OH	1.60e+14	0.	4569
41.	C7H16+OH=C7H15+H2O	1.70e+13	0.	957
42.	C7H15=CH3+C3H6+C3H6	3.70e+13	0.	28708

43. O2+M=O+O+M
44. CH3+H=CH4
45. CH4+H=CH3+H2
46. CH4+O=CH3+OH
47. CH4+OH=CH3+H2O
48. CH4+O2=CH3+HO2
49. CO+O+M=CO2+M
50. CO+O2=CO2+O
51. CH2+H=CH+H2
52. CH2+O=CO+H+H
53. CH2+O2=CO2+H+H
54. CH2+CH3=C2H4+H
55. CH+O=CO+H
56. CH+O2=CO+OH
57. CH3+CH3=C2H6
58. CH3+CH3=C2H5+H
59. C2H6+H=C2H5+H2
60. C2H6+0=C2H5+OH
61. C2H6+OH=C2H5+H2O
62. C2H5+O2=C2H4+HO2
63. C2H5=C2H4+H
64. C2H4+O=HCO+CH3
65. C2H4+OH=C2H3+H2O
66. C2H4+H=C2H3+H2
67. C2H3+H=C2H2+H2
68. C2H3+O2=C2H2+HO2
69. C2H3=C2H2+H
70. C2H2+OH=CH2CO+H
71. C2H2+O=CH2+CO
72. CH2CO+H=CH3+CO
73. CH2CO+O=HCO+HCO
74. CH2CO+OH=CH2O+HCO
75. CH2CO+M=CH2+CO+M
76. C2H2+O=C2HO+H
77. C2HO+O=CO+CO+H
78. C2HO+H=CH2+CO
79. C2H2+OH=C2H+H2O
80. C2H+O=CO+CH
81. C2H+H2=C2H2+H
82. C2H+O2=CO+HCO
83. C2H5+CH3=C3H8
84. C3H8+H=N*C3H7+H2
85. C3H8+H=I*C3H7+H2
86. C3H8+O=N*C3H7+OH
87. C3H8+O=I*C3H7+OH
88. C3H8+OH=N*C3H7+H2O
89. C3H8+OH=I*C3H7+H2O
90. N*C3H7+H=C3H8
91. I*C3H7+H=C3H8
92. N*C3H7+O2=C3H6+HO2
93. I*C3H7+O2=C3H6+HO2
94. N*C3H7=C2H4+CH3
95. N*C3H7=C3H6+H
96. I*C3H7=C3H6+H

Rate coefficients are in the form $k_j = A_j T^{n_j} \exp(- E_j / RT)$. Units are moles, cubic centimeters, seconds, Kelvins and calories/mole.

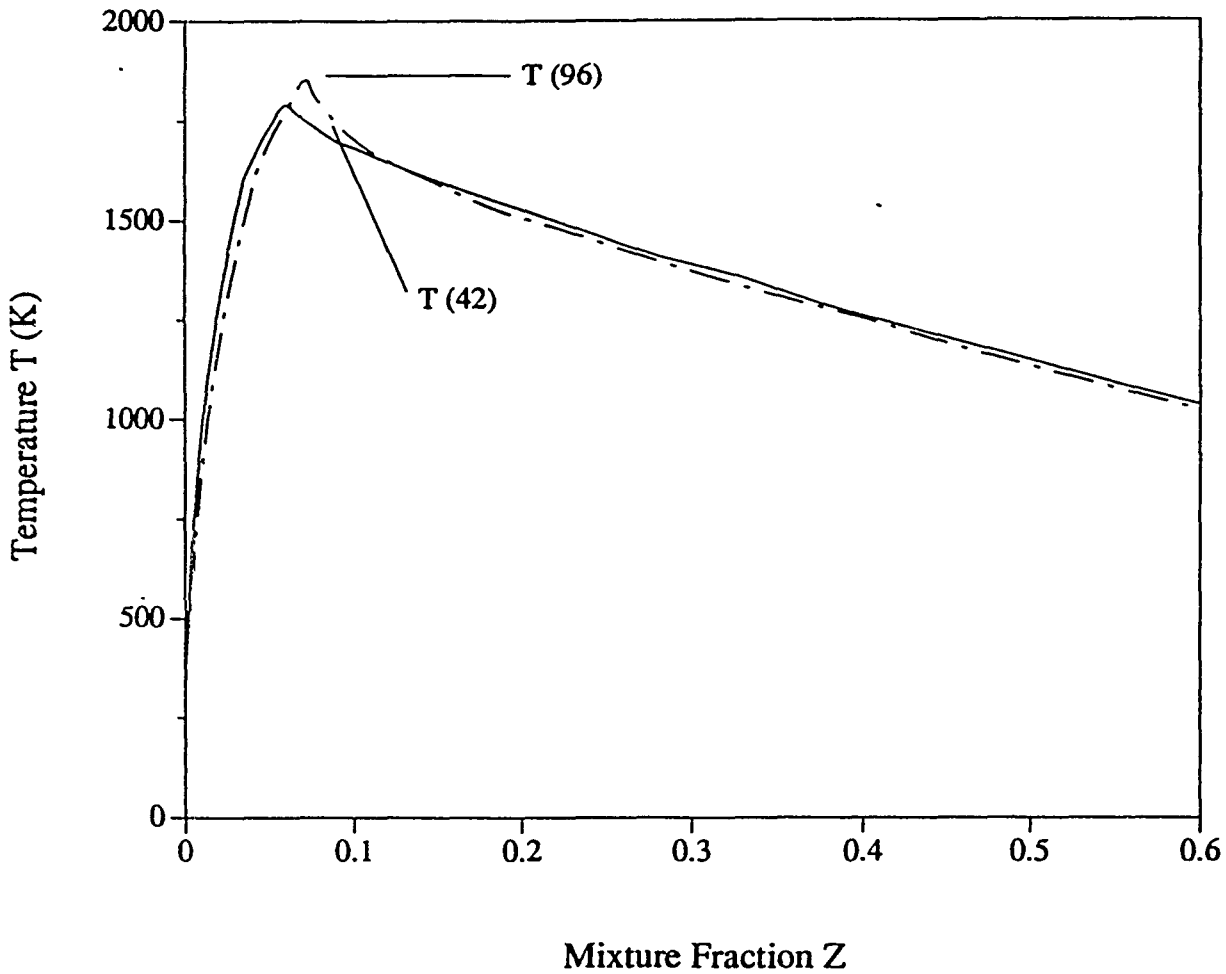

Fig. 1 Comparison between the temperature profile calculated using reactions 1-96 (dashed line) with that calculated using reactions 1-42 (solid line) for a=9.84 s^{-1}

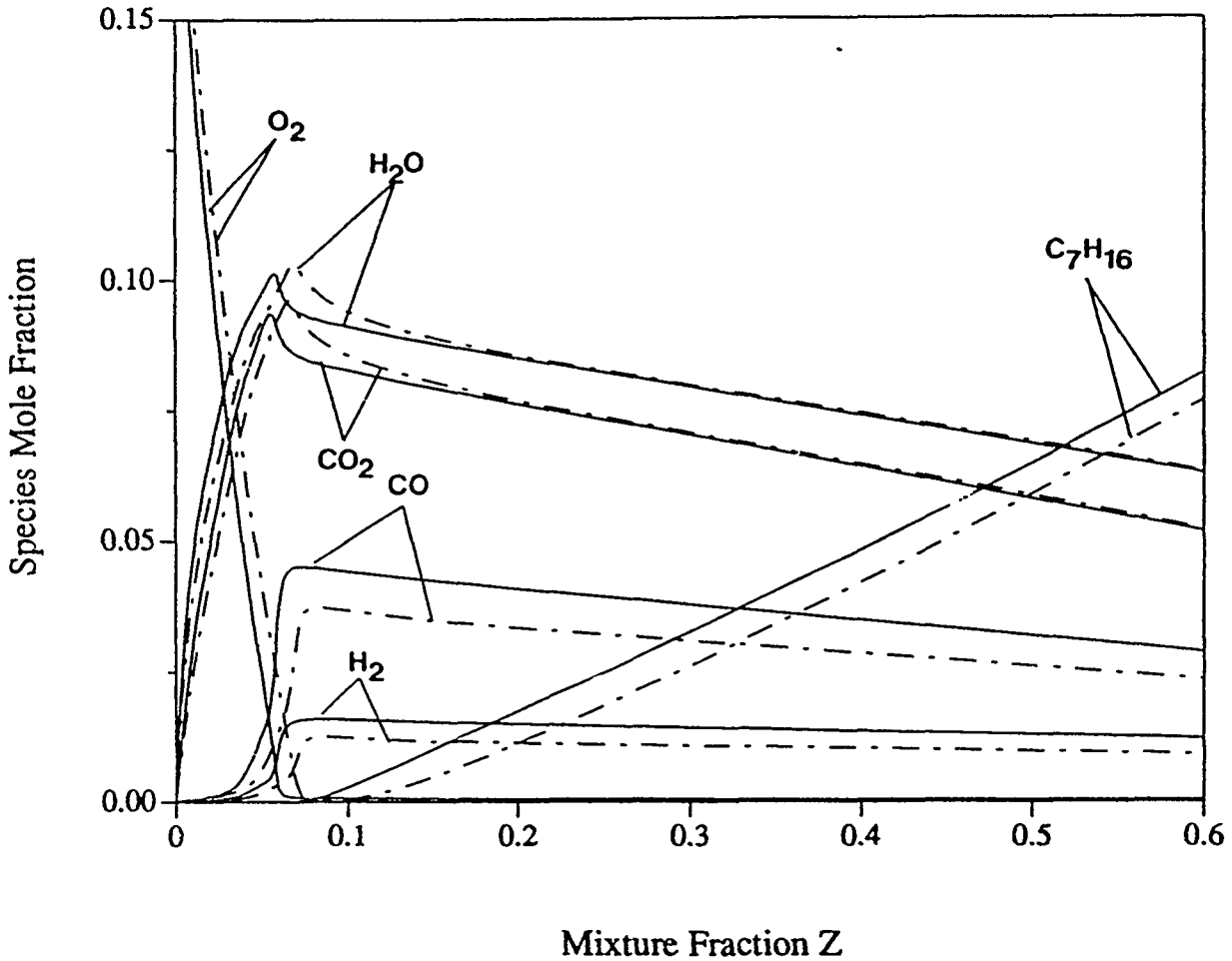

Fig. 2 Comparison between concentration profiles for C_7H_{16}, O_2, CO_2, H_2, CO, and H_2O calculated using reactions 1-96 (dashed lines) with those calculated using reactions 1-42 (solid lines) for $a=9.84\ s^{-1}$

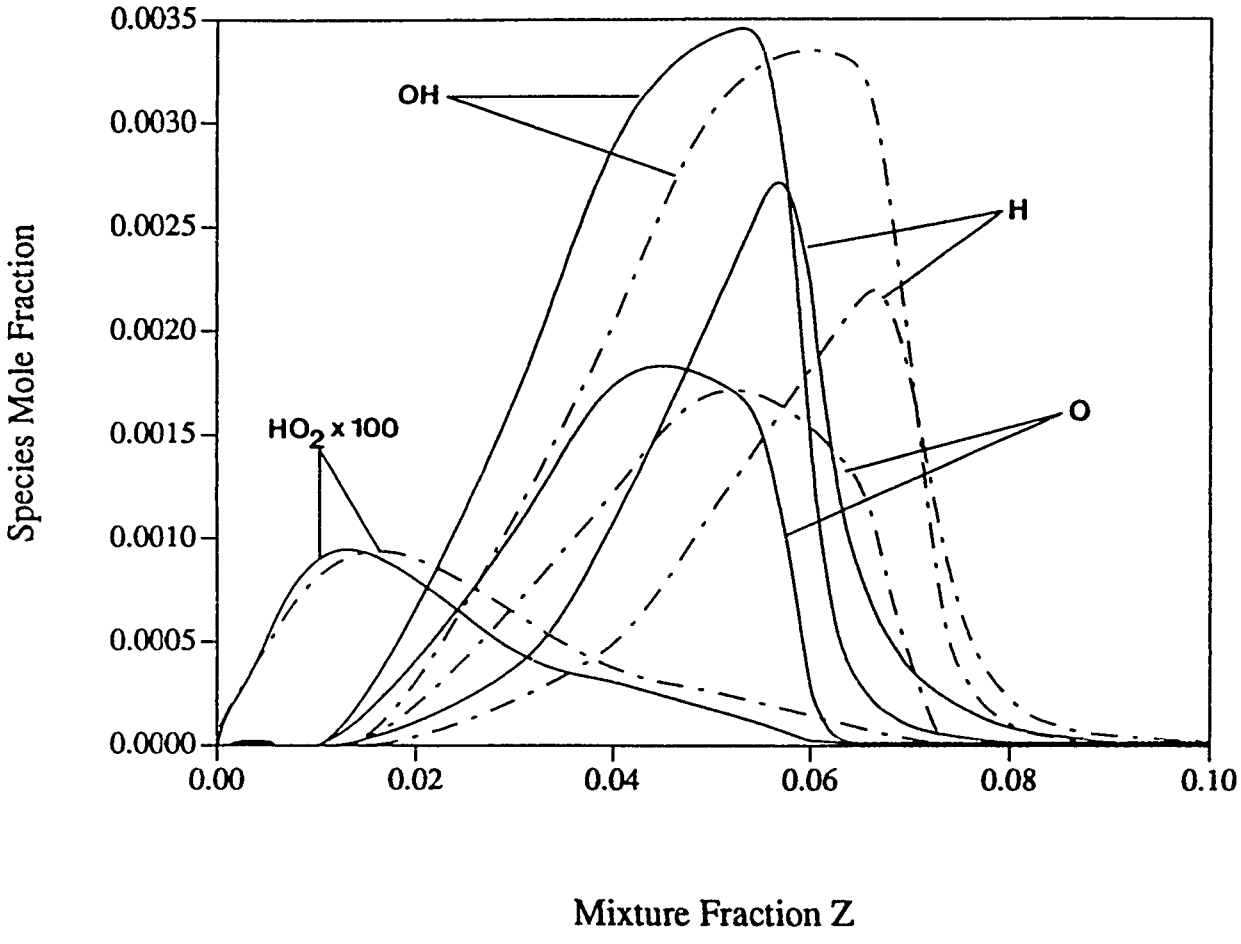

Fig. 3 Comparison between concentration profiles for H, O, OH, and HO_2 calculated using reactions 1-96 (dashed lines) with those calculated using reactions 1-42 (solid lines) for a=9.84 s^{-1}

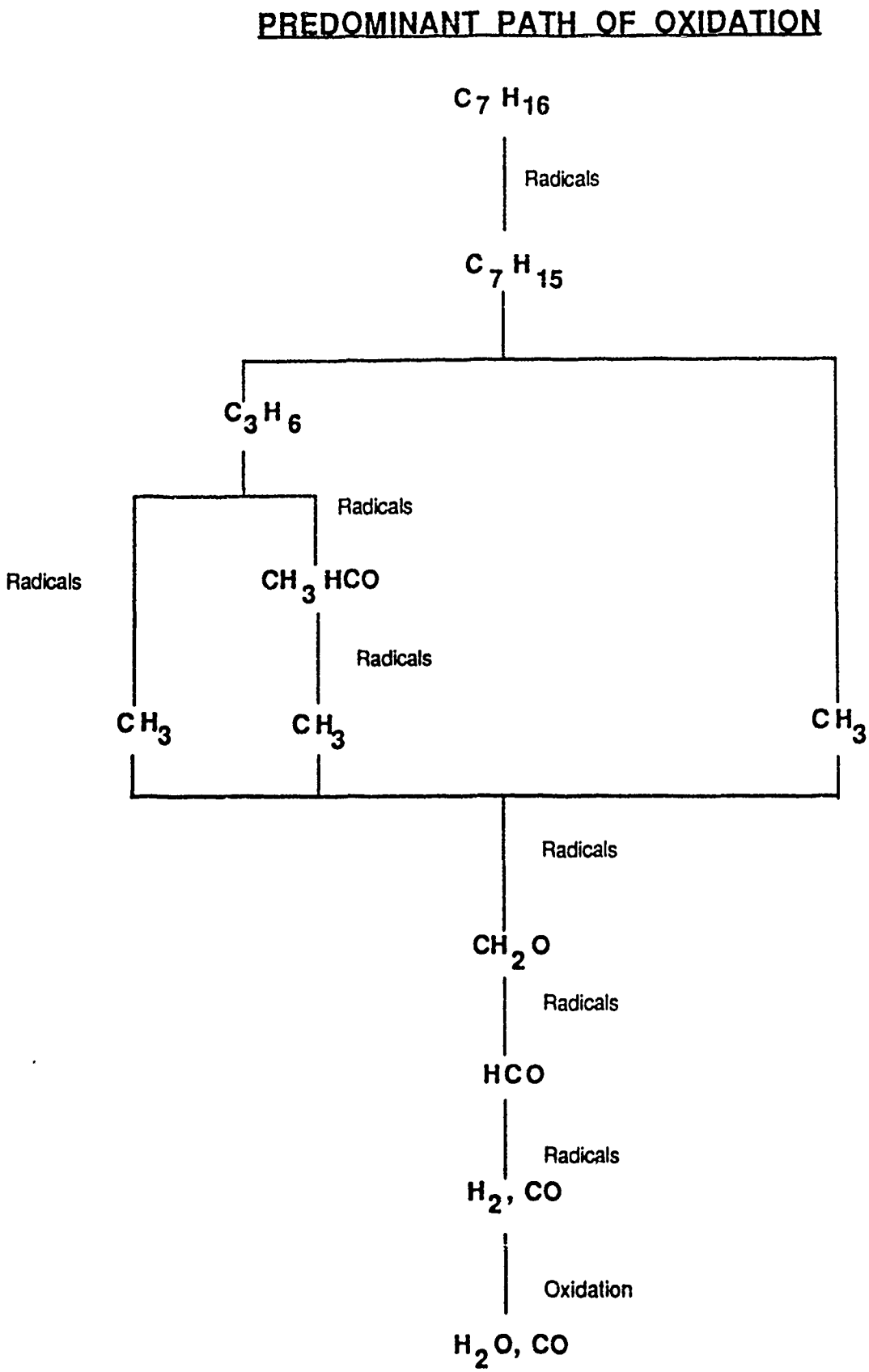

Fig. 4 Schematic illustration of the principal path of oxidation of heptane

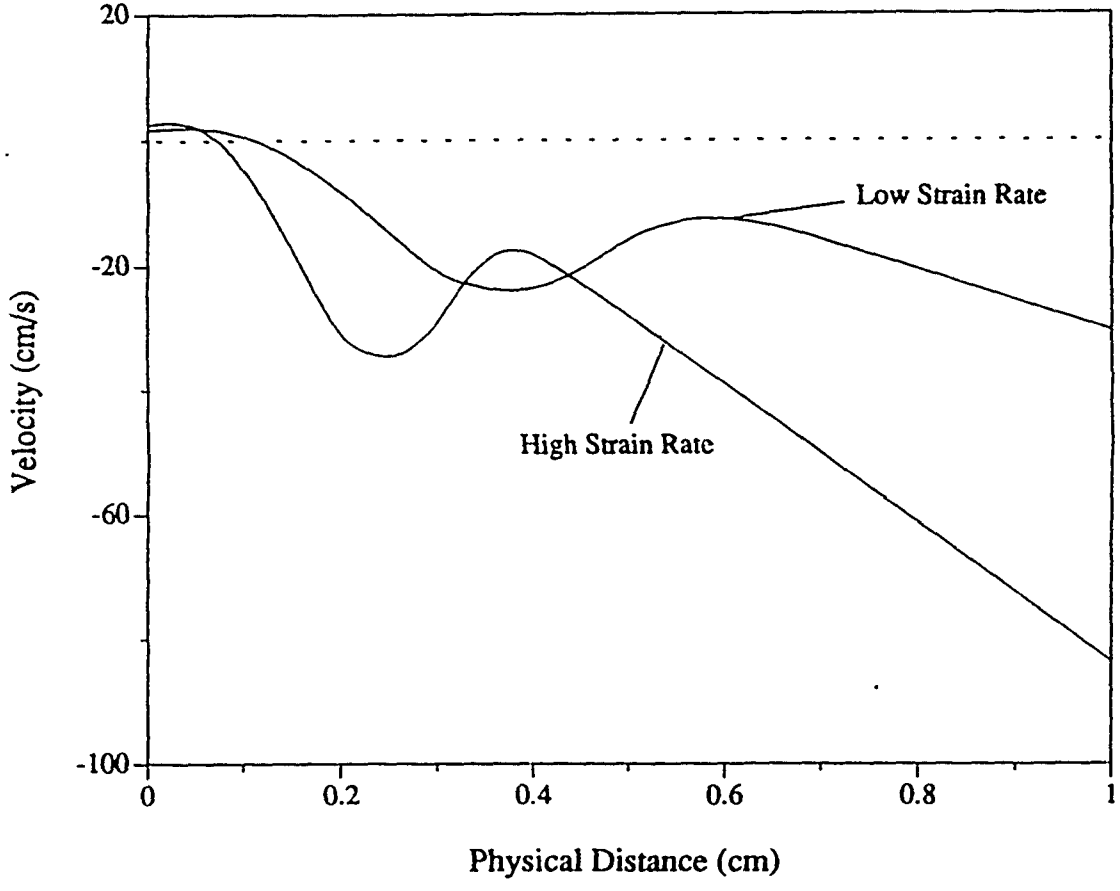

Fig. 5 Calculated profile of the axial component of the velocity for $YO_{2\infty} = 0.185$, U=30.5 cm/s, and U=83.7 cm./s

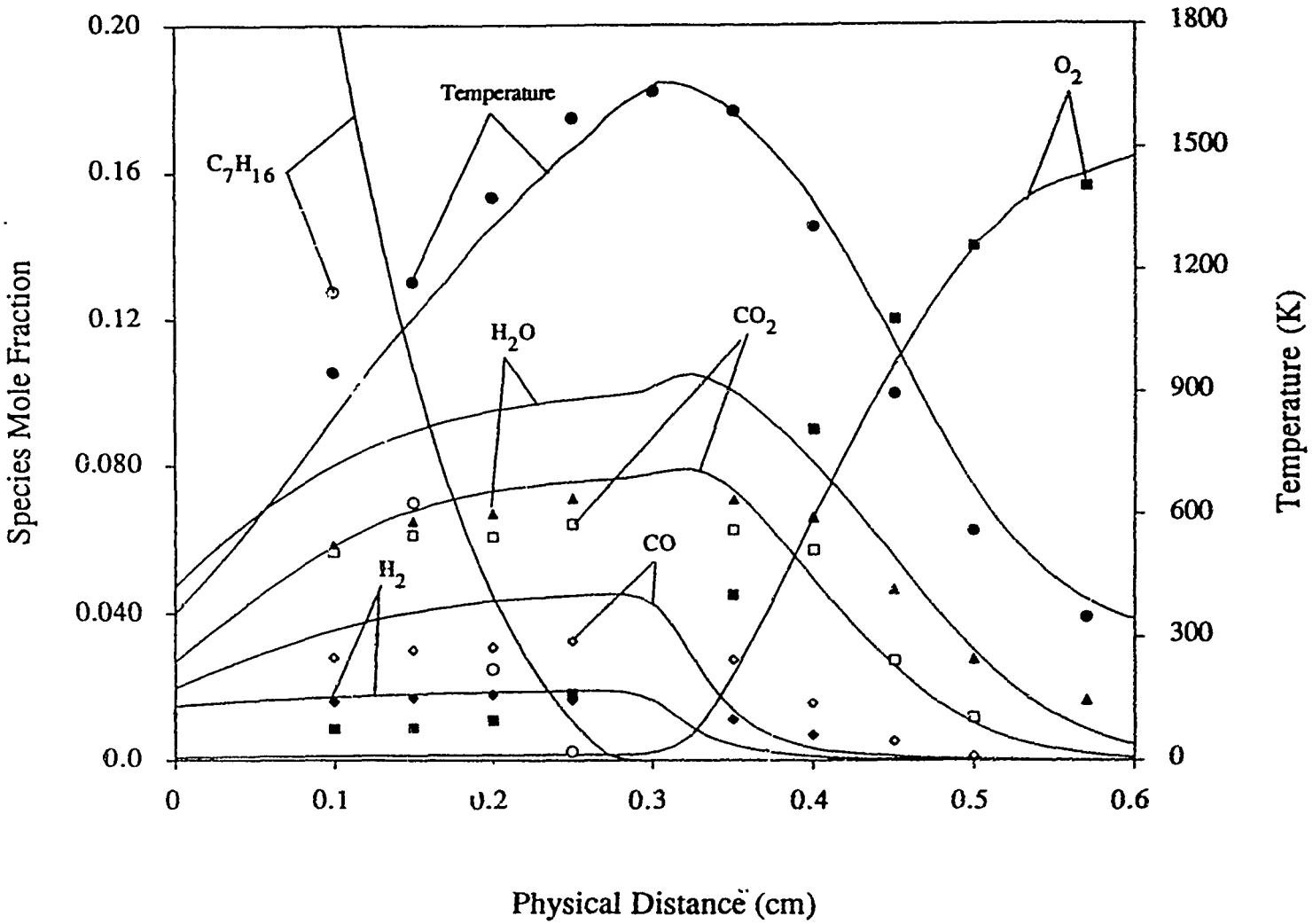

Fig. 6. Comparison between experimental measurements (shown as points) and computed values (lines) for profiles of temperature and stable species: C_7H_{16}, O_2, CO_2, H_2, CO, and H_2O for YO_2 =0.185, U=30.5 cm/s

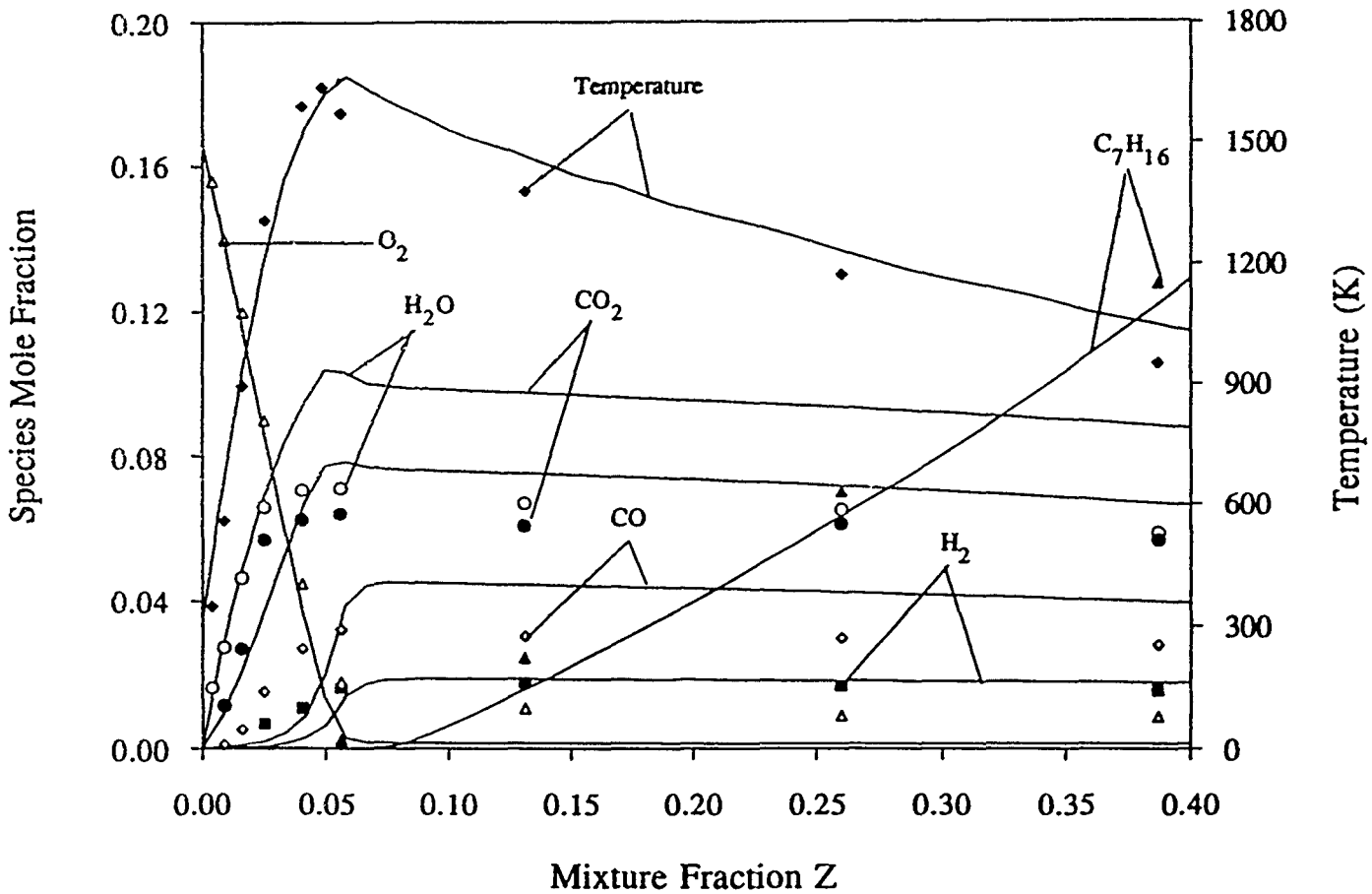

Fig. 7. Comparison between experimental measurements (shown as points) and computed values (lines) for profiles of temperature and stable species: C_7H_{16}, O_2, CO_2, H_2, CO, and H_2O using the mixture fraction Z as the independent variable, for V_{O_2} =0.185, U=30.5 cm/s

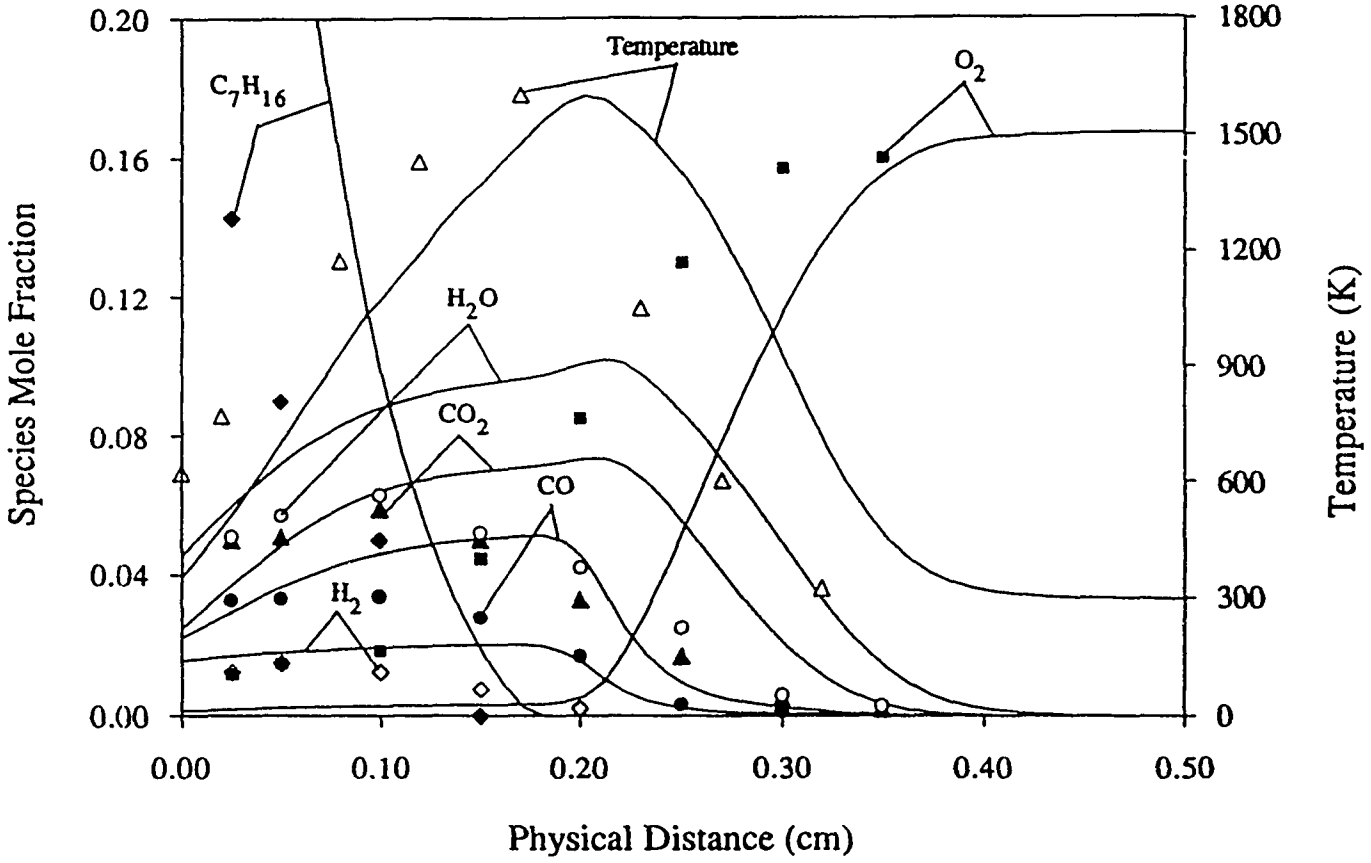

Fig. 8. Comparison between experimental measurements (shown as points) and computed values (lines) for profiles of temperature and stable species: C_7H_{16}, O_2, CO_2, H_2, CO, and H_2O for $YO_{2\infty}$=0.185, U=83.7 cm/s

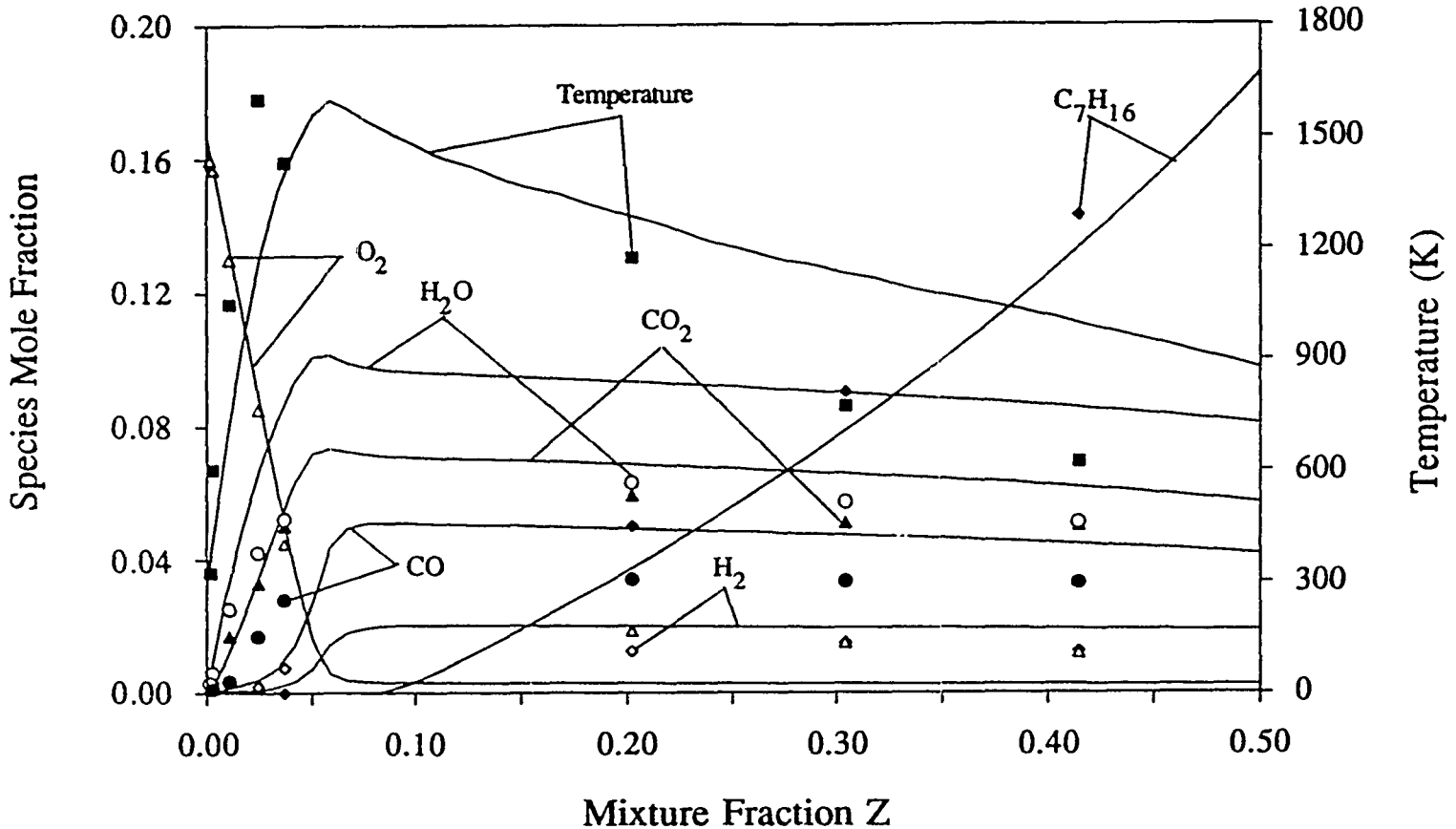

Fig. 9. Comparison between experimental measurements (shown as points) and computed values (lines) for profiles of temperature and stable species: C_7H_{16}, O_2, CO_2, H_2, CO, and H_2O using the mixture fraction Z as the independent variable, for $YO_{2\infty}$=0.185, U=83.7 cm/s

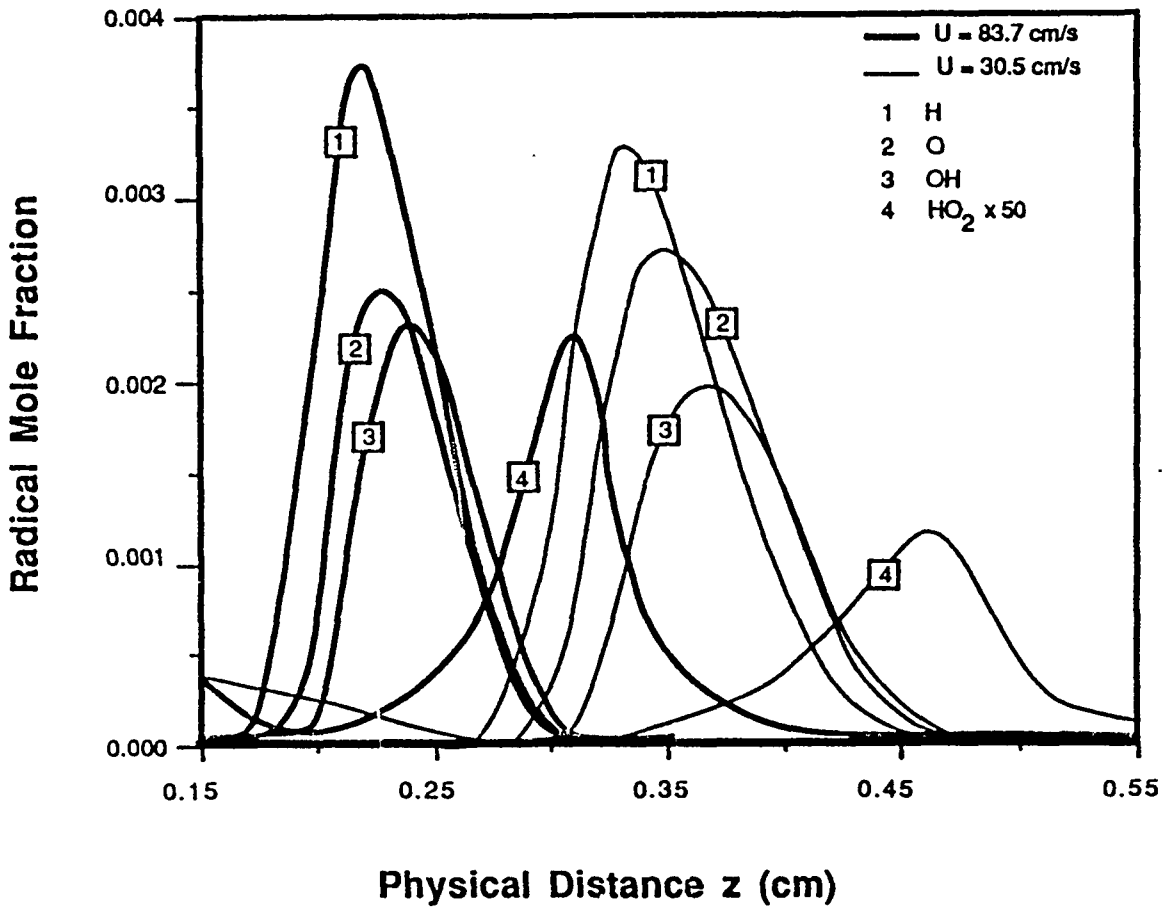

Fig. 10. Calculated profiles for the radicals H, O, OH, and HO_2 for $YO_{2\infty} = 0.185$, U=30.5 cm/s, and U=83.7 cm./s

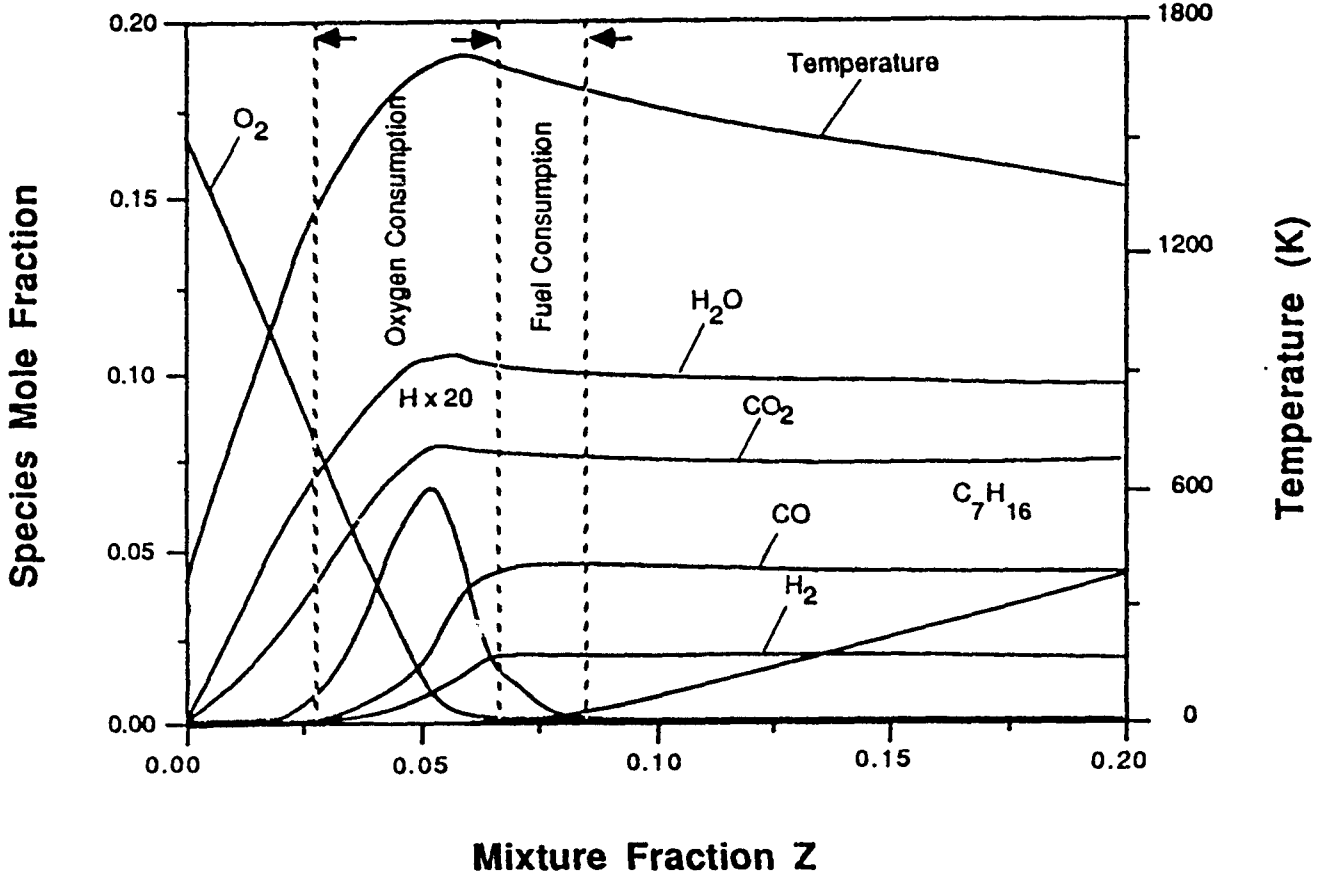

Fig. 11. Aspects of the structure of heptane-air diffusion flames relevant for asymptotic description

Case	Surface Temperature (K)		Maximum Flame Temperature		Flame Stand-off Distance (cm)	
	Experimental	Calculated	Experimental	Calculated	Experimental	Calculated
Y_{O_2} =.185 U = 30.5 cm/s	358	360	1665	1636	.252	.31
Y_{O_2} = .185 U = 83.7 cm/s	356	354	1603	1604	.18	.203

Case	Y_{O_2} at Max. Temperature		Calculated Strain Rate	Calculated Burning Rate	Calculated Z at Surface	Calculated Fuel Mass Fraction at Surface	Calculated $Y_{HO_2\ max}$
	Exp.	Calc.					
Y_{O_2} = .185 U = 30.5 cm/s	.0502	.00363	24.7	.0035	.8264	.813	2.382×10^{-5}
Y_{O_2} = .185 U = 83.7 cm/s	.0914	.0066	55.7	.0054	.8320	.817	4.515×10^{-5}

Table 2 Certain aspects illustrating the influence of strain on structure of heptane-air diffusion flames

CHAPTER III

ANALYSIS OF THE STRUCTURE AND MECHANISMS OF EXTINCTION OF COUNTERFLOW METHANOL-AIR DIFFUSION FLAME

Numerical calculations were performed to determine the structure and to clarify the mechanisms of extinction of diffusion flames stabilized between counterflowing streams of methanol and air. The calculations were performed at a value of the thermodynamic pressure equal to one atmosphere, with different values of the rate of strain , and with two different chemical kinetic mechanisms. We will refer to these two mechanisms as "mechanism a" and "mechanism b". Mechanism a and mechanism b have the same set of elementary reactions, but the rate constants for these elementary reactions were obtained from two different references. Temperature profiles, concentration profiles of various species, rates of production and destruction of various species, and rates of various reactions were plotted as a function of the axial coordinate using mechanism a and mechanism b. Both chemical mechanisms show that the structure can be subdivided into three regions, the fuel consumption region where the reaction proceeds via the path CH_3OH - CH_2OH - CH_2O - CO,H_2; the H_2 - CO oxidation region where the compounds H_2 and CO oxidize to form H_2O and CO_2; and the radical destruction region where radicals are destroyed by three body reactions.

If mechanism a is used, we conclude that at low rates of strain the concentration of CH_2OH and HCO are in steady-state and in partial equilibrium is assumed for certain reactions there exists algebraic relations among the concentrations of the radicals OH, H, and O. As the rate of strain is increased, HCO is no longer in steady-state and no solution was obtained at a value of the strain rate greater than 521 s^{-1}. However, if mechanism b is used, the concentration of only HCO is in steady-state, and there also exist algebraic relations among the concentrations of the radicals OH, H, and O. As the rate of strain is increased, no solution was obtained for a value of the strain rate greater than 168 s^{-1}, and we speculate that extinction of the flame is caused due to a large value of the activation energy for a reaction controlling the pyrolysis of CH_2OH to CH_2O.

The research summarized above has been published in Combustion and Flame 76, pp 111-132, 1989. The coauthors of the publication are Professor C. Trevino, and Professor M. D. Smooke

CHAPTER IV

ASYMPTOTIC STRUCTURE AND EXTINCTION OF METHANE-AIR DIFFUSION FLAMES

The asymptotic structure of a counterflow methane-air flame is analyzed using a three-step chemical kinetic mechanism,

I $CH_4 + O_2 \rightarrow CO + H_2 + H_2O$

II $CO + H_2O \Longleftrightarrow CO_2 + H_2$

III $O_2 + H_2 \rightarrow 2H_2O$

which was deduced in a systematic way through steady state and partial equilibrium assumptions from a detailed chemical kinetic mechanism for oxidation of methane. The rates for the three steps are related to the rates of the elementary reactions . The outer structure of the diffusion flame is the classical Burke-Schumann structure governed by the overall one-step reaction $CH_4 + 2O_2 \rightarrow CO_2 + 2H_2O$, with the flame sheet positioned at $Z = Zst$, where Z is the mixture fraction used as the independent variable in the analysis. The inner structure consists of a thin H_2 - CO oxidation layer of thickness $O(\varepsilon)$ toward the lean side, a thin nonequilibrium layer for the water gas shift reaction of thickness of $O(\nu)$, and a thin fuel consumption layer of thickness $O(\delta)$ toward the rich side. These layers result, respectively, in the limit of large values for the Damkohler number characterizing the rate of reaction III, III, and I, while the ratios of the activation temperature to the gas temperature for the three reactions are assumed to be of order unity. We also find that $\varepsilon > \nu > \delta$. The results of the asymptotic analysis yield values of the temperature and the main species at the fuel consumption layer as a function of the scalar dissipation rate χ_{st}. we therefore obtain the upper branch f the classical S-shaped curve where the maximum flame temperature is plotted as a function of χ_{st}^{-1}. The scalar dissipation rate at quenching χ_q is derived from the S-shaped plot and its relation to the laminar burning velocity is discussed. A comparison of the diffusion flame structure with that of a premixed flame shows that the rich part of the diffusion flame corresponds to the upstream part of the premixed flame while its lean part corresponds to the downstream part. First the kinetic scheme is based on the most important (principal)

reactions to derive the basic structure . When a number of additional elementary chemical reactions are added the results of the asymptotic analysis are found to be in very good agreement with previous numerical calculations that used a complete kinetic mechanism, as well as with experiments.

The research summarized above has been published in Combustion and Flame 73, pp 23 - 44, 1988. The coauthor of this publication is Professor N. Peters. The international collaboration was supported by the National Science Foundation Grant number NSF-INT-86-09939

CHAPTER V. METHANE - AIR PREMIXED FLAMES

V. 1 COMPARISON BETWEEN EXPERIMENTAL MEASUREMENTS AND NUMERICAL CALCULATIONS OF THE STRUCTURE OF COUNTERFLOW, DILUTED, METHANE-AIR, PREMIXED FLAMES.

ABSTRACT

In this chapter results of experimental and numerical study of the structure of premixed flame is reported. The fuel used in this study is gaseous methane. Experiments were performed in premixed flames stabilized between counterflowing streams of a combustible mixture of methane and air diluted with nitrogen and a stream which consists of reaction products from another premixed methane-air flame. Critical conditions of extinction of this flame were measured over a wide parametric range. The detailed structure of the flame was characterized by measuring the concentration profiles of various stable species by removing gas samples from the flame using a quartz microprobe. The gas samples were then analyzed employing gas chromatographic techniques. Temperature profiles were measured by use of coated thermocouples. The measurements were corrected by radiative losses from the thermocouple beads. Detailed numerical calculations were performed to determine the structure of the flame and the results were compared with experimental methods.

It is shown that the basic structure of most hydrocarbon flames including that of methane are similar. Hence, some of the conclusions deduced here can be extended to other premixed flames burning more complex hydrocarbon fuels. Methane was chosen for the present study because gaseous fuels permit experimental measurements to be made over a wide parametric range.

A manuscript describing the research outlined in this chapter will appear in the proceedings of the Twenty-Third (International) Symposium on Combustion, The Combustion Institute 1990. The coauthors of this manuscript are Professor M. D. Smooke, Captain J. Crump, and Dr. V. Giovangigli. The authors acknowledge the invaluable assistance of Dr. Venkat Tangirala with the gas chromatographic measurements. The authors also acknowledge the helpful discussions which they had with Professors F. A. Williams, N. Peters, and P. A. Libby. The research performed at Yale University was supported by the United States Department of Energy and the Air Force Office of Scientific Research.

V.2 THE INNER STRUCTURE OF METHANE-AIR FLAMES

The inner structure of a methane-air premixed flame is analyzed using a reduced four-step chemical kinetic mechanism

$$CH_4 + 2H + H_2O \dashrightarrow CO + 4H_2 \qquad \text{I}$$

$$CO + H_2O \Longleftrightarrow CO_2 + H_2 \qquad \text{II}$$

$$H + H + M \dashrightarrow H_2 + M \qquad \text{III}$$

$$O_2 + 3H_2 \Longleftrightarrow 2H_2O + 2H \qquad \text{IV}$$

The rates of these four steps are related to the rates of elementary reactions appearing in the C_1 chain mechanism for oxidation of methane. The inner layer is thin with reactions I-IV occurring in this layer, and is embedded between a chemically inert upstream layer and a broader (but asymptotically thin) downstream layer where reactions II, III and IV occur and H_2 and CO are oxidized.

The analysis reported here extends a previous analysis by Peters and Williams of the structure of premixed methane - air flames, where a reduced three - step chemical kinetic mechanism was used. In the equations describing the structure of the inner layer a parameter ω appears which represents the ratio of the thickness of the fuel consumption layer to the thickness of the radical consumption layer of the previous analysis by Peters and Williams. Analytical solutions for the burning velocity eigenvalue L are obtained in the limit $\omega \dashrightarrow 0$ and $\omega \dashrightarrow$ infinity, and by use of numerical integration an approximation for L is obtained as a function of ω, which includes limiting expressions for $\omega \dashrightarrow 0$ and $\omega \dashrightarrow$ infinity. The expressions for L contains a number of parameters, which represent the influence of a number of elementary chemical reactions. In particular, a parameter defined as μ in the analysis is found to have a significant influence on the value of L and consequently on the burning velocity, and the influence of this quantity increases with increasing pressure. The parameter μ represents the influence of the backward steps of the reactions $CH_4 + H \Longleftrightarrow CH_3 + H_2$ and $CH_4 + OH \Longleftrightarrow CH_3 + H_2O$.

Using the results of the analysis the burning velocity was calculated for a stoichiometric methane- air flame for values of the pressure p between 1 atm and 80 atm. at p = 1 atm the calculated burning velocity was 38 cm/s in good agreement with experimental results. The burning velocity decreased with increasing pressure again in agreement with experimental measurements.

The research summarized above has been published in Combustion and Flame 81, pp 96-118, 1990. The coauthor of this publication is Professor Norbert Peters.

V.3 THE ASYMPTOTIC STRUCTURE OF NONSTOICHIOMETRIC METHANE-AIR FLAMES

Abstract

The asymptotic structure of methane-air premixed flames is analyzed for all values of the equivalence ratio, using a reduced chemical-kinetic mechanism that can be represented as

I	$CH_4 + 2H + H_2O \rightleftarrows CO + 4H_2$
II	$CO + H_2O \rightleftarrows CO_2 + H_2$
III	$H + H + M \rightarrow H_2 + M$
IV	$O_2 + 3H_2 \rightleftarrows 2H_2O + 2H$

The rates of these four steps are related to the rates of elementary reactions appearing in the C_1-chain mechanism for oxidation of methane. In the analysis the overall flame structure is subdivided into four zones, a preheat zone, an inner layer, a H_2-CO oxidation layer and a post-flame zone. The inner layer is located between the preheat zone and the oxidation layer. The inner layer is thin in comparison to the preheat zone, and in this layer finite-rate reactions related to the consumption of the fuel are considered. Downstream from this inner layer there exists a broader (but asymptotically thin) oxidation layer where reaction II, III and IV occur and H_2 and CO are oxidized to form H_2O and CO_2.

The asymptotic analysis employed for the inner layer is essentially identical to the previous analysis of Seshadri and Peters. However, the analysis of the H_2-CO oxidation layer is different because the values of the concentrations of the species H_2, CO and O_2 are not necessarily negligibly small in the post-flame zone downstream from the oxidation layer. The results of the asymptotic analysis are used to calculate the burning velocity of the flame as a function of the equivalence ratio for various values of the pressure. An apparent overall activation energy is deduced from the analysis, and the corresponding Zel'dovich number increases rapidly as the equivalence ratio departs from unity. The large

value of the Zel'dovich number for very fuel-rich and very fuel-lean flames makes these flames much more sensitive to heat loss or flame stretch. This result, coupled with the finding from the analysis that a fundamental chemical-kinetic mechanism for extinction does not exist at the experimentally observed flammability limits, suggests that flammability limits are due to heat losses for methane-air flames.

1. Introduction

The asymptotic structure of stoichiometric, laminar, premixed methane-air flames has been investigated previously [1,2] using a reduced chemical-kinetic mechanism to describe the gas-phase oxidation of this fuel. This reduced mechanism was deduced systematically from a detailed chemical-kinetic mechanism by assuming that the concentrations of a number of intermediate species are in a dynamic steady state [3]. In the analysis of Peters and Williams [1], a three-step mechanism was employed, and an asymptotic analysis was performed using only the principal elementary reactions to characterize the overall rates of the reduced mechanism. Results for the burning velocity as a function of pressure and orders of magnitude of the concentrations of all intermediates were obtained [1]. The results of the asymptotic analysis were improved by including a number of additional chemical reactions in the overall rates of the reduced mechanism through numerical evaluation of an integral involving an iteration for determination of the integrand. In the analysis of Seshadri and Peters [2], a four-step mechanism was used, and the effects of additional reactions were represented by additional algebraic parameters to avoid the iteration of Ref. 1, which would be inapplicable with the four-step mechanism. Results were obtained for the burning velocity of the flame for values of pressure p including the range 1 atm to 40 atm, addressed here. At p = 1 atm the calculated burning velocity was 35 cm/s, in reasonable agreement with experimental results [2]. The burning velocity decreased with increasing pressure, again in agreement with experimental measurements.

Here the analyses reported in Refs. 1 and 2 are extended to all values of the equivalence ratio ϕ. Only terms of leading order in the asymptotics are retained because the

contributions of the higher-order terms have been estimated to be 20% or less, comparable with inaccuracies introduced by other approximations in the analysis. The intent is to illustrate the character of the analysis and of the results and to provide an indication of the errors that may be expected from the asymptotics at leading order. Investigation of the greater accuracy that can be achieved by proceeding to higher order is not an objective of the present paper. Owing to the neglect of C_2 chemistry, the results of the analysis are expected to be notably inaccurate for fuel-rich flames, and therefore potential improvements in the asymptotics for fuel-rich conditions are not thoroughly explored. The asymptotic analysis and notation used here closely follow the development in Ref. 2.

2. Structure of the Post-Flame Zone

Downstream of the flame, in the post-flame zone the reaction products are in chemical equilibrium, and the temperature is equal to the adiabatic flame temperature. The equilibrium concentrations of the products are determined as described elsewhere [4] by assuming that only the species O_2, H_2, CO, CO_2 and H_2O are present and are in chemical equilibrium, and that the enthalpy and the element mass fractions are equal to those in the unburnt gas. For given values of ϕ, p and the initial temperature, T_u, the adiabatic flame temperature, T_b, and the mass fraction of species i in the post-flame zone, Y_{ib}, can be calculated. The equivalence ratio is related to the mixture fraction Z by

$$\phi = \frac{Z}{Z_{st}} \frac{(1 - Z_{st})}{(1 - Z)}, \tag{1}$$

where $Z_{st} = 0.055$ is the stoichiometric mixture fraction. In Fig. 1 results of thermochemical calculations are plotted showing the conditions in the post-flame zone as functions of ϕ.

Shown in Fig. 1a, in addition to T_b, is the adiabatic flame temperature T_c for complete combustion with $Y_{H_2} = Y_{CO} = 0$, which corresponds to the overall reaction $CH_4 + 2O_2 \rightarrow CO_2 + 2H_2O$. In this limit the products would contain unburnt O_2 for fuel-

lean flames and unburnt CH_4 for fuel-rich flames. If the heat of combustion for this overall reaction per mole of CH_4 consumed is denoted by $(-\Delta H)$, then

$$\int_{T_u}^{T_c} c_{p,P} dT = \begin{cases} (-\Delta H) Y_{Fu}/W_F & \text{for } \phi \le 1 \\ (-\Delta H) Y_{O_2u}/(2W_O) & \text{for } \phi \ge 1 \end{cases}$$

where $c_{p,P}$ is the specific heat at constant pressure of the product mixture (N_2, CO_2, H_2O and O_2 or CH_4), Y_{Fu} and Y_{O_2u} denote the mass fractions of fuel and oxidizer, respectively, in the initial reactant stream, and W_i is the molecular weight of species i. Figure 1 shows that the discontinuity in slope at $\phi = 1$, predicted by this formula, is smoothed when the equilibrium chemistry is considered, and there is a region in which the products contain O_2, H_2 and CO simultaneously. Expansions later will be performed about T_c rather than T_b.

3. Reduced Chemical-Kinetic Mechanism

A chemical-kinetic mechanism describing the oxidation of methane is shown in Table 1. The rate parameters here differ somewhat from those employed in Ref. 1 but are the same as those of Ref. 2 and are obtained from a recent [5] reevaluation of the rate data. Employing the procedure described in Ref. 6, a four-step mechanism can be deduced from this mechanism by assuming that there exists a dynamic steady state for the concentrations of the species O, OH, HO_2, H_2O_2, CH_3, CH_2O, CH_3O and HCO. The four-step mechanism can be written as

I	$CH_4 + 2H + H_2O \rightleftarrows CO + 4H_2,$
II	$CO + H_2O \rightleftarrows CO_2 + H_2,$
III	$H + H + M \rightarrow H_2 + M,$
IV	$O_2 + 3H_2 \rightleftarrows 2H_2O + 2H.$

The reaction rates w_k, k = I, II, III, IV for the overall reactions I – IV can be related to the reaction rates of the elementary reactions w_n, n = 1,2, ..., 25 shown in Table 1 and are

$$\left.\begin{aligned} w_I &= w_{10f} - w_{10b} + w_{11f} - w_{11b} + w_{12f} - w_{12b}, \\ w_{II} &= w_{9f} - w_{9b}, \\ w_{III} &= w_5 - w_{10f} + w_{10b} + w_{16} - w_{18} + w_{19} - w_{22f} + w_{22b} + w_{24} + w_{25}, \\ w_{IV} &= w_{1f} - w_{1b} + w_6 + w_{18} + w_{22f} - w_{22b}, \end{aligned}\right\} \quad (2)$$

where the subscripts f and b identify forward and backward rates, respectively. The values of the reaction rates w_n shown in Eq. (2) are proportional to the product of the concentration of the reactants and the rate constant k_n of the elementary reaction. Results of numerical calculations have shown that reactions 10f, 19, 21, 22f, 22b, 23f and 23b have only a minor influence on the burning velocity of premixed flames; therefore, as in Ref. 2, they are neglected in the analysis reported here. In addition to the steady-state assumptions, as in previous analyses [1,2], the elementary reaction 3 shown in Table 1 is assumed to be in equilibrium yielding the algebraic relation $C_{OH} = \gamma C_H$, where C_i is the molar concentration of species i and

$$\gamma \equiv \frac{C_{H_2O}}{K_3 C_{H_2}} \quad (3)$$

in which $K_3 = 0.23 \exp(7530/T)$ is the equilibrium constant of the elementary reaction 3.

4. The Conservation Equations for a Steady Premixed Flame

For a steady, planar, adiabatic deflagration at low Mach number the equation of motion implies that the pressure is essentially constant. The equation for mass conservation can be written as

$$\rho v = \rho_u v_u, \quad (4)$$

where ρ is the density and v the gas velocity. The index u denotes conditions in the unburnt gas. Lewis numbers for species i are defined as $L_i = \lambda/(\rho c_p D_i)$, where λ is the

thermal conductivity and c_p is the mean specific heat; the diffusion coefficient D_i is taken to be that of species i with respect to nitrogen, and the binary-diffusion approximation is employed. The values of the Lewis numbers for all species are assumed to be constant. Using the notation of the previous analysis [1,2], the non-dimensionalized species and energy balance equations can be written as

$$\left.\begin{aligned} \mathcal{L}_F(X_F) &= -\omega_I, \\ \mathcal{L}_H(X_H) &= -2\omega_I - 2\omega_{III} + 2\omega_{IV}, \\ \mathcal{L}_{H_2}(X_{H_2}) &= 4\omega_I + \omega_{II} + \omega_{III} - 3\omega_{IV}, \\ \mathcal{L}_{H_2O}(X_{H_2O}) &= -\omega_I - \omega_{II} + 2\omega_{IV}, \\ \mathcal{L}_{O_2}(X_{O_2}) &= -\omega_{IV}, \\ \mathcal{L}_{CO}(X_{CO}) &= \omega_I - \omega_{II}, \\ \mathcal{L}_{CO_2}(X_{CO_2}) &= \omega_{II}, \\ \mathcal{L}(\tau) &= Q_I\omega_I + Q_{II}\omega_{II} + Q_{III}\omega_{III} + Q_{IV}\omega_{VI}. \end{aligned}\right\} \qquad (5)$$

The operators are defined as $\mathcal{L}_i \equiv d/dx - (1/L_i)d^2/dx^2$, and $\mathcal{L} = d/dx - d^2/dx^2$. The non-dimensional independent variable x is related to the spatial coordinate x′ as $x = \int_0^{x'} (\rho v c_p/\lambda)dx'$, and the quantities X_i and τ are related to the mass fraction of species i, Y_i and the gas temperature, T as

$$X_i = \frac{Y_i W_F}{Y_{Fu} W_i}, \qquad \tau = \frac{T - T_u}{T_c - T_u}, \qquad (6)$$

where the subscript F denotes the fuel. In the analysis the average molecular weight $\overline{W}$ is assumed to be a constant equal to 27.62 kg/kmol; hence X_i is the mole fraction of species i divided by the initial mole fraction of the fuel. The non-dimensionalized reaction rates ω_k and the non-dimensionalized heats of reaction Q_k of the reduced four-step mechanism are defined as

$$\omega_k = \frac{\lambda W_F w_k}{c_p Y_{Fu}(\rho_u v_u)^2}, \qquad Q_k = \frac{Y_{Fu}(-\Delta H_k)}{c_p(T_c - T_u) W_F}. \qquad (7)$$

The non-dimensionalization of Eq. (7) will also be applied to the rates of the elementary steps. Since assuming steady states and negligible concentrations for CO, H_2 and H enables the overall reaction $CH_4 + 2O_2 \rightarrow CO_2 + 2H_2O$ to be deduced from the four-step mechanism by adding twice reaction IV to the sum of reactions I, II and III, it follows from the definition of Q_k given in Eq. (7) that $Q_I + Q_{II} + Q_{III} + 2Q_{IV} = 1$.

A schematic illustration of the presumed structure of the premixed flame is shown in Fig. 2. It consists of a chemically inert preheat zone, followed by the inner layer, the H_2-CO oxidation layer and the equilibrium post-flame zone. The structures of the inner layer and the oxidation layer are similar to those shown in Ref. 2. In the inner layer all the hydrocarbon chemistry occurs, resulting in the formation of H_2 and CO as well as some H_2O and CO_2. In the oxidation layer H_2 and CO are oxidized to form H_2O and CO_2. The concentration of fuel is zero in the oxidation layer, and the H-radicals are in steady state. In the post-flame zone downstream of the H_2-CO oxidation layer, H_2 and CO are in partial equilibrium according to reaction II. However, there exists a sublayer between the inner layer and the oxidation layer where reaction II is not in equilibrium.

5. Asymptotic Analysis of the Inner Layer

Since the asymptotic analysis of the inner layer is identical to that of Ref. 2, only the results of the previous analysis will be shown here. The thickness of this layer is presumed to be of order δ, where

$$\delta = \left[\frac{k_{1f} k_{13}'' X_{O_2}}{k_{11f}' k_{13}' L_F} \right]^0, \tag{8}$$

in which the superscript 0 implies that these quantities are evaluated at the origin, $x = 0$, which is taken to coincide with the location of the inner layer, and at this point $T = T^0$ and $X_i = X_i^0$. Other quantities in Eq. 8 are

$$\left.\begin{aligned} k_{13}'' &\equiv k_{13}' + \left[\left(k_{2f}' k_{10b} + \gamma k_{1b} k_{11b}'\right)/k_{1f}\right](C_{H_2}/C_{O_2}), \\ k_{11f}' &\equiv k_{11f} + \gamma k_{12f}, \\ k_{13}' &\equiv k_{13} + \gamma k_{18}/K_1, \\ k_{2f}' &\equiv k_{2f} + \gamma K_3 k_{4b}, \\ k_{11b}' &\equiv k_{11b} + \gamma K_3 k_{12b}. \end{aligned}\right\} \tag{9}$$

The value of $X_{O_2}^0$ is of order ε, where ε is a measure of the thickness of the H_2-CO oxidation layer. In addition, the ratio k_{1f}/k_{11f}' is small, and k_{13}''/k_{13}' is roughly of order unity; hence δ will be presumed to be smaller than ε, and the ordering $\delta << \varepsilon$ used in the previous analyses [1,2] is retained here.

Following the analysis in Ref. 2 a quantity L which contains the burning velocity is defined as

$$L \equiv A\delta^2\left(k_{11f}' k_{13}'/k_{13}''\right)^0 L_F R^0, \tag{10}$$

where

$$\left.\begin{aligned} A &\equiv \frac{Y_{F_u}}{v_u^2 W_F}\left[\frac{\lambda}{c_p}\right]^0\left[\frac{T_u}{T^0}\right]^2, \\ R &\equiv \left\{\frac{k_{1f} k_{2f}' X_{O_2} X_{H_2}}{\gamma k_{1b}\left[\gamma k_{2b}' + (\gamma k_{24} + k_{25}) C_M\right]}\right\}^{1/2} \\ k_{2b}' &\equiv k_{2b} + \gamma k_{4f}. \end{aligned}\right\} \tag{11}$$

The concentration of the third body C_M appearing in Eq. (11) can be written in terms of the chaperon efficiency η_i of species i (i = 1, ... N) as $C_M = \left[p\overline{W}/(\hat{R}T)\right]\sum_{i=1}^{N} \eta_i Y_i/W_i$, where the gas constant is $\hat{R}$ = 82.05 atm cm^3/(mol K), and p is in atmospheres. In the previous analysis [2] two limiting structures for the inner layer were identified depending on the value of a parameter ω defined as

$$\omega = 2\delta L_H/R^0. \tag{12}$$

The quantity ω represents the ratio of the thickness of the fuel-consumption layer (of order δ), where the reaction I is presumed to occur, to the thickness of the radical-consumption layer of the previous analysis [1].

A schematic illustration of the presumed structure of the inner layer in the limit $\omega \to 0$, and $L/\omega = O(1)$ is shown in Fig. 3a [2]. The fuel-consumption reaction I will occur in a thin layer of thickness of order $\delta\omega^{-2/3}$, which for convenience is presumed to be located at $\zeta = x/\delta = 0$. The structure of this layer resembles that of a diffusion flame into which fuel diffuses from one side and H-radicals from the other. Outside this diffusion layer in the region of positive x there exists a radical nonequilibrium layer of thickness of order $\delta\omega^{-1}$, where the concentration of fuel is zero. From analyzing the structure of the diffusion-flame layer shown in Fig. 3a it can be shown [2] that the quantity L is given by the expression

$$L_0 = 2\omega\left(1 + 2\kappa + 4\theta/3 + 8\psi/15 + 2\sigma\right), \tag{13}$$

where

$$\left.\begin{aligned} \kappa \equiv \left[\frac{k_5 C_M(k_7 + \gamma k_8)}{k_{1f}(k_6 + k_7 + \gamma k_8)}\right]^0, \qquad \theta \equiv \left[\frac{\gamma k_{1b}\kappa}{k'_{2f}X_{H_2}} + \frac{(\gamma k_{24} + k_{25})C_M}{k_{1f}X_{O_2}}\right]^0 R^0, \\ \psi \equiv \left[\frac{\gamma k_{1b}R}{k'_{2f}X_{H_2}}\right]^0, \qquad \sigma \equiv \left[\frac{k'_{2f}k_{10b}X_{H_2} - 2\gamma k_{1b}k_{18}X_{O_2}}{k_{1f}k'_{13}X_{O_2}}\right]^0. \end{aligned}\right\} \tag{14}$$

A schematic illustration of the presumed structure of the inner layer in the limit $\omega \to \infty$ with $L = O(1)$ is shown in Fig. 3b. Here, the fuel consumption reaction I occurs in a relatively broad layer, and embedded in this layer is a thin layer, of thickness of order

$\delta\omega^{-1/3}$, where reaction IV is not equilibrium. Asymptotic analysis of the structure of this layer shows that [2]

$$L_\infty^{-1} = \frac{8}{15}\left[\left\{1+\frac{5}{2}\kappa+\frac{15}{16}\theta+\frac{5}{8}\psi+\frac{5}{8}\chi+2\sigma+\frac{15}{4}\mu\left[\frac{3-4\beta^2+\beta^4}{\beta^4}\ln(1+\beta)\right.\right.\right.$$
$$\left.\left.\left.-\frac{2\beta^4-4\beta^3-9\beta^2+3\beta+6}{2\beta^3(1+\beta)}\right]\right\}^{-1}-\mu(\ln\mu+\ln E_\mu+\tilde{C}-1)\right]. \qquad (15)$$

The various parameters appearing in Eq. (15) are defined as

$$\left.\begin{aligned}\beta &\equiv \left[\frac{\gamma k_{2b}' k_{13} R}{k_{1f} k_{13}' X_{O_2}}\right]^0, \quad \mu \equiv \left[\frac{k_{2f}' k_{11b}' X_{H_2}^2}{k_{1f} k_{13}'' X_{O_2} R}\right]^0\left[1+\frac{k_{18} X_{O_2}}{k_{11b}' X_{H_2}}\right]^0,\\ \chi &\equiv \left[\frac{k_{16} R Y_{Fu} \overline{W}}{k_{17} W_F}\right]^0,\\ E_\mu &\equiv \frac{\left(E_{11b}+n_{11b}\hat{R}T_r+E_{2f}+n_{2f}\hat{R}T_r-E_{1f}\right)\delta(T_c-T_u)\tau^0}{\hat{R}T^{0\,2}},\end{aligned}\right\} \qquad (16)$$

where E_n and n_n refer, respectively, to the activation energy and the temperature exponent of the frequency factor of the elementary chemical reaction n shown in Table 1, T_r being the reference temperature, set equal to 1600 K [1,2], and $\tilde{C} = 0.5772$ is Euler's constant.

An ad-hoc approximation to determine L for all values of ω has been proposed and tested previously [2] and is given by the expression

$$L = L_\infty\left[1-\left(1+\frac{L_0}{0.18L_\infty}\right)^{-0.18}\right]. \qquad (17)$$

Equation (17) will be used with the equations derived from analyzing the structure of the H_2-CO oxidation layer to calculate the burning velocity of the flame.

6. Analysis of the H_2-CO Oxidation Layer

The burning velocity v_u can be calculated from Eqs. (8)-(17) if T^0, $X_{H_2}^0$, $X_{O_2}^0$ and $X_{H_2O}^0$ are known. To determine these quantities the structure of the H_2-CO oxidation layer

downstream from the inner layer must be analyzed. In this layer simplifications to the conservation equations arise because convection can be neglected in the first approximation and $X_F = 0$; hence $\omega_I = 0$. The H radicals are presumed to be in steady state in this layer, whence from Eq. (5) $\omega_{III} = \omega_{IV}$. It can then be shown [2] that for small θ and κ, X_H is given by the expression

$$X_H = R\left(1 - \theta/2 - \kappa/2\right). \tag{18}$$

The water-gas shift reaction II is presumed to be in partial equilibrium everywhere in this layer except in a thin non-equilibrium sublayer adjacent the inner layer. Following the development in Refs. 1 and 2, the structure of the oxidation layer will first be analyzed by assuming that reaction II is in equilibrium everywhere, and later corrections to the value of $X^0_{H_2}$ and X^0_{CO} introduced by non-equilibrium of reaction II will be obtained. Equilibrium of reaction II implies that there exists an algebraic relation between the concentrations of H_2 and CO that can be written as

$$x_{CO} = \alpha x_{H_2}, \tag{19}$$

where

$$\alpha \equiv K_3 X_{CO_2} L_{H_2} / (K_9 X_{H_2O} L_{CO}), \quad x_i \equiv X_i / L_i, \tag{20}$$

in which $K_9 = 0.0096 \exp(11623/T)$ is the equilibrium constant of elementary reaction 9. The partial-equilibrium assumptions make it necessary to eliminate ω_{II} from Eqs. (5). With $\omega_{III} = \omega_{IV}$ and the neglect of the convective terms in Eqs. (5) the expressions

$$\left.\begin{aligned} \frac{d^2}{dx^2}[(1+\alpha)x_{H_2}] &= 2\omega_{III}, \\ \frac{d^2}{dx^2}[x_{H_2} + x_{H_2O}] &= 0, \\ \frac{d^2}{dx^2}[(1+\alpha)x_{H_2} - 2x_{O_2}] &= 0, \\ \frac{d^2}{dx^2}\left[\left(Q^*_{III}/2 + \alpha Q^*_{III}/2 + \alpha Q_{II}\right)x_{H_2} + \tau\right] &= 0, \end{aligned}\right\} \tag{21}$$

are obtained, where $Q^*_{III} = Q_{III} + Q_{IV}$. Since the numerical values $Q^*_{III}/2 = 0.3116$ and $Q^*_{III}/2 + Q_{II} = 0.3479$, obtained from thermochemical tables, are sufficiently close, they can be replaced by their arithmetic mean, $q \equiv Q^*_{III}/2 \approx Q^*_{III}/2 + Q_{II} \approx 0.33$. The expansions

$$\left.\begin{aligned} 2qx &= \varepsilon\eta, \quad \tau = \tau_b - \varepsilon z, \quad q(1+\alpha)x_{H_2} = \varepsilon(b+z), \\ 2qx_{O_2} &= \varepsilon(a+z), \quad x_i = x_{ib} - \varepsilon z_i, \qquad i = H_2O,\ CO_2, \end{aligned}\right\} \tag{22}$$

are then introduced, where $\tau_b \equiv (T_b - T_u)/(T_c - T_u)$, $b \equiv q(1+\alpha)X_{H_2b}/(\varepsilon L_{H_2})$, $a \equiv 2qX_{O_2b}/(\varepsilon L_{O_2})$, in which ε is presumed to be a small quantity, and η, z, a, b, α, z_i, τ_b and τ are order of unity.

Under the assumption that $(\gamma k_{24} + k_{25})C_M/(\gamma k'_{2b})$ is small, an expression for the R of Eq. (11) may be obtained from Eqs. (3) and (22) and substituted into Eq. (18) to show that X_H can be expressed as

$$X_H = \frac{\varepsilon^2 K_1^{1/2} K_2^{1/2} K_3 L_{H_2}^{3/2} L_{O_2}^{1/2} (z+b)^{3/2}(z+a)^{1/2}}{2^{1/2} q^2 X_{H_2O}(1+\alpha)^{3/2}} \left[1 - \frac{\theta}{2} - \frac{\kappa}{2}\right], \tag{23}$$

where $K_1 = 12.7 \exp(-8108/T)$ and $K_2 = 2.25 \exp(-1040/T)$ are the equilibrium constants of elementary reactions 1 and 2, respectively. The source term ω_{III} in Eq. (21) can be written from Eqs. (2) and (7) in terms of the expansions shown in Eqs. (22) as

$$\omega_{III} = 2q\varepsilon^3 D_{III}\left[G_{III}(z+a)^{3/2}(z+b)^{3/2} + G'_{III}S^0(z+a)(z+b)^2\right], \tag{24}$$

where

$$
\left.
\begin{aligned}
D_{III} &= \frac{A(k_5 C_M)^0 \left(K_1^{1/2} K_2^{1/2} K_3\right)^0 (L_{H_2} L_{O_2})^{3/2} (1 - \kappa/2 - \theta/2)}{2^{5/2} q^4 X_{H_2O}^0 (1 + \alpha^0)^{3/2}}, \\
S &= \frac{(2K_1 K_2 L_{H_2})^{1/2} (1 - \kappa/2 - \theta/2)(k_{24} + k_{25}/\gamma)}{k_5 (1 + \alpha)^{1/2} L_{O_2}^{1/2}}, \\
G_{III} &= \frac{(k_5 C_M)\left(K_3 K_1^{1/2} K_2^{1/2}\right) X_{H_2O}^0 (1 + \alpha^0)^{3/2} (\lambda/c_p)}{(k_5 C_M)^0 \left(K_3 K_1^{1/2} K_2^{1/2}\right)^0 X_{H_2O} (1 + \alpha)^{3/2} (\lambda/c_p)^0} \left[\frac{T^0}{T}\right]^2, \\
G'_{III} &= \frac{(K_1 K_2)^{1/2} (k_{24} + k_{25}/\gamma)\, k_5^0 (1 + \alpha^0)^{1/2}}{\left[(K_1 K_2)^{1/2}\right]^0 (k_{24} + k_{25}/\gamma)^0 k_5 (1 + \alpha)^{1/2}} G_{III}.
\end{aligned}
\right\} \qquad (25)
$$

In the inner layer $G_{III} = G'_{III} = 1$, and following previous analysis [1,2] the quantity ε will be presumed to be

$$\varepsilon = D_{III}^{-1/4}. \qquad (26)$$

Introduction of Eq. (22) into Eq. (21), followed by use of Eqs. (24)-(26) with $G_{III} = G'_{III} = 1$, results in the leading-order problem

$$
\left.
\begin{aligned}
&\frac{d^2 z}{d\eta^2} = (z + a)^{3/2} (z + b)^{3/2} + S^0 (z + a)(z + b)^2, \\
&\frac{dz}{d\eta} = -1 \text{ at } \eta = 0, \qquad \frac{dz}{d\eta} \to 0 \text{ as } \eta \to \infty,
\end{aligned}
\right\} \qquad (27)
$$

which implies that

$$2\int_0^{z^0} \left[(z + a)^{3/2} (z + b)^{3/2} + S^0 (z + a)(z + b)^2\right] dz = 1. \qquad (28)$$

Here $\alpha = \alpha^0$ is employed in the definition of b so that, like a and S^0, this parameter may be treated as constant in performing the integration. It can be easily verified that if a = b = 0. then this problem reduces to the leading-order problem considered earlier [1,2].

The solution to Eq. (28) for z^0 as a function of a, b and S^0 must be obtained numerically. For a given value of ϕ, thermochemical calculations would yield the values of T_b, X_{O_2b}, X_{H_2b}, X_{COb}, X_{CO_2b} and X_{H_2Ob}. The quantities a and b depend on ε, which may be expressed as a function of T^0 according to

$$\varepsilon = \frac{T_b - T^0}{z^0(T_c - T_u)}. \tag{29}$$

In addition, S^0 depends on T^0; hence all parameters in Eq. (28) depend on results from the structure of the inner layer. Before calculating the burning velocity, corrections to $x^0_{H_2}$ resulting from non-equilibrium of reaction II in the sublayer adjacent to the inner layer must be obtained [1,2]. In this layer the influence of reactions III and IV can be neglected. Introducing the expansions

$$x = \nu\tilde{\zeta}, \quad X_{H_2} = X^0_{H_2} + \nu L_{H_2}\tilde{z}_{H_2}, \quad X_{CO} = X^0_{CO} + \nu L_{CO}\tilde{z}_{CO}, \tag{30}$$

where

$$\nu = \frac{\varepsilon^{3/2}(k_5 C_M)^{0^{1/2}} K_3^{0^{1/2}} L_{H_2}^{1/2} L_{O_2}^{1/2}(1 - \kappa/2 - \theta/2)^{1/2}}{2k_{9f}^{0^{1/2}} X_{H_2O}^{0^{1/2}} q^{3/2} L_{CO}^{1/2}(z^0 + b)^{1/4}(z^0 + a)^{1/4}(1 + \alpha^0)^{1/2}}, \tag{31}$$

it can be shown following previous [1,2] methods that the solution in the non-equilibrium sublayer can be written as

$$\left.\begin{aligned} \tilde{z}_{H_2} &= -\frac{1 - \alpha^0}{(1 + \alpha^0)^{3/2}} \exp\left[-(1 + \alpha^0)^{1/2}\tilde{\zeta}\right] - \frac{2\tilde{\zeta}}{1 + \alpha^0} \\ \tilde{z}_{CO} &= -\frac{1 - \alpha^0}{(1 + \alpha^0)^{3/2}} \exp\left[-(1 + \alpha^0)^{1/2}\tilde{\zeta}\right] - \frac{2\,\alpha^0\tilde{\zeta}}{1 + \alpha^0}. \end{aligned}\right\} \tag{32}$$

At the inner layer $\tilde{\zeta} = 0$; hence

$$x^0_{H_2} = \frac{\varepsilon(z^0+b)}{q(1+\alpha^0)}\left[1+\frac{\nu q(1+\alpha^0)}{\varepsilon(z^0+b)}\tilde{z}^0_{H_2}\right] = \frac{\varepsilon(z^0+b)}{q(1+\alpha^0)}\left[1 - \varepsilon^{1/2}\frac{(k_5C_M)^{0'^2}(1-\alpha^0)K_3^{0'^2}L_{H_2}^{1/2}L_{O_2}^{1/2}(1-\kappa/2-\theta/2)^{1/2}}{2k_{9f}^{0'^2}X_{H_2O}^{0'^2}(1+\alpha^0)q^{1/2}L_{CO}^{1/2}(z^0+b)^{5/4}(z+a)^{1/4}}\right], \tag{33}$$

which can be used in the expression

$$L = \frac{k_{1f}^{0^2}k_{13}^{''0}L_{O_2}(1+\alpha^0)^{3/2}(z^0+a)^{5/2}(x^0_{H_2}q/\varepsilon)^{3/2}}{(k_5C_M)^0k_{11f}^{'0}k_{13}^{'0}L_F(1-\kappa/2-\theta/2)}, \tag{34}$$

obtained with the aid of Eqs. (8), (10), (11) and (23). By use of Eq. (33), Eq. (34) expresses L in terms of T^0 and z^0, since ε is related to T^0 as shown in Eq. (29). Since Eq. (17) provides an independent expression for L as a function of T^0, the quantities T^0 and z^0 can both be calculated numerically when Eq. (28) is integrated. In view of Eqs. (26) and (29), the burning velocity can then be calculated by rewriting the first of Eqs. (11) and (25) as

$$v_u^2 = \frac{Y_{Fu}}{W_F}\left[\frac{\lambda}{c_p}\right]^0\left[\frac{T_u}{T^0}\right]^2\frac{(k_5C_M)^0\left(K_1^{1/2}K_2^{1/2}K_3\right)^0(L_{H_2}L_{O_2})^{3/2}(1-\kappa/2-\theta/2)(T_b-T^0)^4}{2^{5/2}q^4X^0_{H_2O}(1+\alpha^0)^{3/2}(T_c-T_u)^4z^{0^4}}. \tag{35}$$

7. Results and Discussions

Equation (35) was used by the procedure described above to calculate the burning velocity as a function of the equivalence ratio, initial temperature, and pressure. In these calculations the value of λ/c_p appearing in Eq. (35) was expressed as $\lambda/c_p = 2.58 \times 10^{-4}\,(T/298)^{0.7}$ g/(cm s). The Lewis numbers for the various species were presumed to be constant, with $L_F = 0.97$, $L_{O_2} = 1.1$, $L_{H_2O} = 0.83$, $L_{CO_2} = 1.39$, $L_{H_2} = 0.3$, $L_H = 0.18$ and $L_{CO} = 1.11$. Calculations were performed for values of ϕ between 0.5 and 1.55, for values of p between 1 atm to 40 atm, and for $T_u = 300$ K and $T_u = 600$ K.

Figure 4 shows results of numerical solution of Eq. (28) for the value of z^0 at the inner layer, and the values of a and b. The rapid decreases of a on the rich side and of b on the lean side show that the concentration of oxygen in the post-flame zone is small for rich flames, and the concentration of hydrogen in the post-flame zone is small for lean flames. Figure 5 shows the values of L and ω as functions of ϕ, demonstrating that ω decreases with increasing ϕ. For fuel-lean flames, where the value of ω is large, the value of L is given approximately by Eq. (15), and for fuel-rich flames, where the value of ω is small, L is given approximately by Eq. (13). It has been shown previously [2] that for stoichiometric flames the value of L decreases and the value of ω increases with increasing pressure. Hence, the expression for L given by Eq. (15) becomes more accurate for fuel-lean flames at high pressure, and the structure of such flames would resemble that shown in Fig. 3b. Equation (13) would become more accurate for fuel-rich flames at low pressure, and the structures of such flames resemble that shown in Fig. 3a. However, for fuel-rich flames, because of various uncertainties in the analysis, such as questions concerning our neglect of C_2 chemistry in the chemical-kinetic mechanism shown in Table 1, the extent of occurrence of the diffusion-flame layer requires further study.

In Fig. 6, the variations of κ, θ and σ with ϕ are shown, and in Fig. 7 the variations of δ, ν and ε, which represent the thicknesses of the various layers shown in Figs. 2, 3a and 3b, are plotted as functions of ϕ. The former shows the current expansions, treating κ, θ and σ as small, are reasonably accurate except for rich flames, and the latter shows the relative orderings to be reasonable, except that ν is not small compared with ε, so that water-gas nonequilibrium should be considered throughout the ε layer for greater accuracy. At p = 1 atm, the values of ψ and χ are not small [2], so there is some inaccuracy in the expansions in Eqs. (13) and (15), although the effects tend to be mitigated by other terms; at high p these inaccuracies disappear. In Fig. 8 the temperature in the inner layer T^0 is

plotted as a function of ϕ. The value of T^0 increases with increasing values of ϕ and approaches T_b for very fuel-rich and very fuel-lean flames. Since Eq. (35) shows that the burning velocity is proportional to $(T_b - T^0)^4$, the burning velocity must become small for highly fuel-rich or fuel-lean flames.

In Figs. 9 and 10 the burning velocity v_u is plotted as a function of ϕ for various values of p, for T_u = 300 K and for T_u = 600 K, respectively. For p = 1 atm and T_u = 300 K, the solid curves in Fig. 9 indicate that the burning velocity reaches a maximum value of approximately 36 cm/s at $\phi \approx 1.1$. Full numerical calculations using somewhat different rate data [7] gave quite similar results, except that the maximum burning velocity was much closer to the accepted maximum of about 43 cm/s. A similar observation applies for the numerical calculations with the rate data of Table 1, as shown in Fig. 9. In addition, it is seen in Fig. 9 that for p = 1 atm, ϕ = 1 and T_u = 300 K, the value $v_u \approx 33$ cm/s, found here by the asymptotic analysis, lies below the value obtained from detailed numerical calculations employing the same rate parameters, but the agreement improves greatly at lean conditions and at higher pressures. As the pressure increases, the peak value of v_u obtained from the asymptotics occurs at decreasing values of ϕ, but always greater than unity, in agreement with numerical and experimental results.

The qualitative features of the behavior of v_u with ϕ and p for T_u = 600 K shown in Fig. 10 are similar to those for T_u = 300 K shown in Fig. 9, but the values of v_u for given values of ϕ and p are higher for T_u = 600 as is expected. It is interesting to note that for both values of T_u solutions were obtained for values of ϕ beyond the reported [8,9] rich and lean flammability limits. Therefore the results of the analysis indicate that there does not exist a chemical-kinetic mechanism for flame extinction and that the experimentally observed flammability limits must be influenced by heat losses.

The small discontinuity in slope at ϕ = 1, seen in Figs. 9 and 10 as well as in various other curves, is a consequence of the expansion about T_c in the analysis of the layer of CO

and H_2 oxidation. Figure 1a shows the discontinuity in the slope of T_c that is responsible for this behavior. The discontinuity involves terms of order ε in the analysis of the oxidation layer, and it can be removed by alternative treatments of this layer. For example, expansions can be pursued about T_b instead of T_c, with x_{H_2} (and consequently x_{CO}) treated as being of order unity in Eq. (22), instead of being of order ε. Because of the magnitude of ε, seen in Fig. 7, these different approaches give results differing by amounts on the order of 20%, as has been verified in the present study by pursuit of alternative analyses not reported here. The discontinuity was retained in the present paper to help to illustrate better what types and magnitudes of inaccuracies may be anticipated from the asymptotic treatment. Future research could be directed towards seeking optimum approaches to the analysis of the oxidation layer, with higher-order terms in ε considered and with improved treatments of water-gas nonequilibrium.

It has been shown previously [1,2] that an effective activation energy E_{eff} may be obtained by fitting v_u to an Arrhenius form in T_b. Hence, if $E_{eff} \equiv 2\hat{R}T_b^2 d[\ln(\rho_u v_u)]/dT_b$, then from differentiation of Eq. (35) with respect to T_b under the assumptions that T^0 is independent of T_b and that T_b equals T_c, the relationship

$$E_{eff} = \frac{4\hat{R}T_b^2}{T_b - T_u}\left[\frac{T^0 - T_u}{T_b - T^0} + \frac{dT_u}{dT_b}\right] \tag{36}$$

is obtained. If the quantity dT_u/dT_b is neglected, an effective Zel'dovich number [3] can then be defined as

$$Ze = \frac{E_{eff}(T_b - T_u)^2}{\hat{R}T_b^2(T^0 - T_u)} = \frac{4}{\varepsilon z^0}, \tag{37}$$

where use was made of Eq. (29). In Fig. 11, this Ze is plotted as a function of ϕ for various values of p at $T_u = 300$ K. Interestingly, the value of Ze is a minimum at $\phi = 1.0$, and increases rapidly with increasing or decreasing values of ϕ. In addition, the minimum value of the Ze increases with increasing values of p. The large value of Ze near the experimentally observed flammability limits implies that the flame is extremely sensitive to heat losses, and hence it would be increasingly difficult to obtain a steady flame

propagation in increasingly fuel-lean or fuel-rich mixtures. These observations could bear on why flammability limits are observed in experiments. It must be emphasized, as discussed in Ref. 1, that the large value of the Zel'dovich number obtained here is related to T^0, which is determined by the relative rates of important elementary reactions, and is unrelated to one-step activation-energy asymptotics.

8. Conclusions

This paper extends the asymptotic analysis of methane flames initiated in [1] and [2] by considering off-stoichiometric conditions. It shows that such an analysis in principle can be done but that many parameters enter into the formulation. Nevertheless, the essence of the structure originally proposed in [1] remains valid in the entire range of equivalence ratios and pressures considered here. A particularly useful result is the possibility of defining and calculating an effective Zel'dovich number and thereby establishing a link to previous large-activation-energy analyses.

Acknowledgements

The research described in this chapter is being prepared for publication. We thank Dr. B. Rogg of Cambridge University for many valuable suggestions and Mr. F. Mauss of RWTH Aachen for providing the numerical results shown in Fig. 9. This research was partially supported by the U.S. National Science Foundation through Grant Number CTS-8918527. The international collaboration was partially supported by the U.S. National Science Foundation Grant number NSF-INT-86-09939. The coauthors of this publication are Mr. J. Goettgens, Professors N. Peters and F.A. Williams.

References

1. Peters, N., and Williams, F.A., *Combust. Flame* 68 (1987) 185-207.

2. Seshadri, K., and Peters, N. "The Inner Structure of Methane-Air Flames", to appear in *Combust. Flame* (1989).

3. Williams, F.A., *Combustion Theory*, 2nd Edition, Addison-Wesley Publishing Company (1985).

4. Kennel, C., Göttgens, J., and Peters, N., "The Basic Structure of Lean Propane Flames", Twenty-Third Symposium (International) on Combustion, The Combustion Institute, Pittsburgh, to appear, 1991.

5. Smooke, M.D., ed., *Reduced Kinetic Mechanisms and Asymptotic Approximations for Methane-Air Flames*, Springer-Verlag, to appear, 1990.

6. Peters, N., *Numerical Simulation of Combustion Phenomena* (R. Glowinski, B. Larroutusiou and R. Temam, Eds.) Lecture Notes in Physics 241, Springer Verlag (1985) 90-109.

7. Warnatz, J., *Eighteenth Symposium (International) on Combustion*, The Combustion Institute, Pittsburgh, 1981, pp. 369-384.

8. Glassman, I., *Combustion*, 2nd Edition, Academic Press (1987).

9. Coward, H.F., and Jones, G.W., Limits of Flammability of Gases and Vapors, Bulletin 503, Bureau of Mines, U.S. Government Printing Office, Washington, D.C., 1952.

List of Tables and Figures

Table 1 The elementary reaction mechanism and associated rate coefficients.

Fig. 1 Results of thermochemical calculations showing the conditions in the burnt gas zone of the flame at p = 1 atm and T_u = 300 K for (a) temperatures and (b) mass fractions.

Fig. 2 A schematic illustration of the overall flame structure.

Fig. 3 A schematic illustration of the inner layer in the limit (a) $\omega \to 0$, $L/\omega = O(1)$ and (b) $\omega \to \infty$, $L = O(1)$.

Fig. 4 Results of numerical calculations showing z^0, a and b as functions of ϕ for p = 1 atm and T_u = 300 K.

Fig. 5 Variation of the parameters L and ω with the equivalence ratio ϕ for p = 1 atm and T_u = 300 K.

Fig. 6 Variation of the parameters θ, σ and κ with ϕ for p = 1 atm and T_u = 300 K.

Fig. 7 Variation of the quantities δ, ν and ε with ϕ for p = 1 atm and T_u = 300 K.

Fig. 8 Variation of the temperature at the inner layer T^0 with ϕ for various values of the pressure p, and for T_u = 300 K.

Fig. 9 The burning velocity v_u as a function of ϕ for various values of the pressure p at T_u = 300 K from the present theory (lines) and from numerical integrations using the mechanism of Table 1 for p = 1, 5 and 20 atm (points).

Fig. 10 The burning velocity v_u as a function of ϕ for various values of the pressure p at T_u = 600 K.

Fig. 11 Variation in the value of the effective Zel'dovich number with ϕ for various values of p at T_u = 300 K.

Table 1

Chemical kinetic mechanism

Number	Reaction	A_n	n_n	E_n
$1f$	$H + O_2 \rightarrow O + OH$	2.0×10^{14}	0.0	16800
$1b$	$O + OH \rightarrow O_2 + H$	1.575×10^{13}	0.0	690
$2f$	$O + H_2 \rightarrow OH + H$	1.8×10^{10}	1.0	8826
$2b$	$OH + H \rightarrow O + H_2$	8.0×10^{9}	1.0	6760
$3f$	$H_2 + OH \rightarrow H_2O + H$	1.17×10^{9}	1.3	3626
$3b$	$H_2O + H \rightarrow H_2 + OH$	5.09×10^{9}	1.3	18588
$4f$	$OH + OH \rightarrow H_2O + O$	6.0×10^{8}	1.3	0
$4b$	$H_2O + O \rightarrow OH + OH$	5.9×10^{9}	1.3	17029
5	$H + O_2 + M^a \rightarrow HO_2 + M^a$	2.3×10^{18}	−0.8	0
6	$H + HO_2 \rightarrow OH + OH$	1.5×10^{14}	0.0	1004
7	$H + HO_2 \rightarrow H_2 + O_2$	2.5×10^{13}	0.0	700
8	$OH + HO_2 \rightarrow H_2O + O_2$	2.0×10^{13}	0.0	1000
$9f$	$CO + OH \rightarrow CO_2 + H$	1.51×10^{7}	1.3	−758
$9b$	$CO_2 + H \rightarrow CO + OH$	1.57×10^{9}	1.3	22337
$10f$	CH_4 (+ M)$^b \rightarrow CH_3 + H$ (+ M)^b	6.3×10^{14}	0.0	104000
$10b$	$CH_3 + H$ (+ M)$^b \rightarrow CH_4$ (+ M)^b	5.20×10^{12}	0.0	−1310
$11f$	$CH_4 + H \rightarrow CH_3 + H_2$	2.2×10^{4}	3.0	8750
$11b$	$CH_3 + H_2 \rightarrow CH_4 + H$	9.57×10^{2}	3.0	8750
$12f$	$CH_4 + OH \rightarrow CH_3 + H_2O$	1.6×10^{6}	2.1	2460
$12b$	$CH_3 + H_2O \rightarrow CH_4 + OH$	3.02×10^{5}	2.1	17422
13	$CH_3 + O \rightarrow CH_2O + H$	6.8×10^{13}	0.0	0
14	$CH_2O + H \rightarrow HCO + H_2$	2.5×10^{13}	0.0	3991
15	$CH_2O + OH \rightarrow HCO + H_2O$	3.0×10^{13}	0.0	1195
16	$HCO + H \rightarrow CO + H_2$	4.0×10^{13}	0.0	0
17	$HCO + M \rightarrow CO + H + M$	1.6×10^{14}	0.0	14700
18	$CH_3 + O_2 \rightarrow CH_3O + O$	7.0×10^{12}	0.0	25652
19	$CH_3O + H \rightarrow CH_2O + H_2$	2.0×10^{13}	0.0	0
20	$CH_3O + M \rightarrow CH_2O + H + M$	2.4×10^{13}	0.0	28812
21	$HO_2 + HO_2 \rightarrow H_2O_2 + O_2$	2.0×10^{12}	0.0	0
$22f$	$H_2O_2 + M \rightarrow OH + OH + M$	1.3×10^{17}	0.0	45500
$22b$	$OH + OH + M \rightarrow H_2O_2 + M$	9.86×10^{14}	0.0	−5070
$23f$	$H_2O_2 + OH \rightarrow H_2O + HO_2$	1.0×10^{13}	0.0	1800
$23b$	$H_2O + HO_2 \rightarrow H_2O_2 + OH$	2.86×10^{13}	0.0	32790
24	$OH + H + M^a \rightarrow H_2O + M^a$	2.2×10^{22}	−2.0	0
25	$H + H + M^a \rightarrow H_2 + M^a$	1.8×10^{18}	−1.0	0

Rate constants are $k_n = A_n T^{n_n} \exp(-E_n/(RT))$; units are moles, cubic centimeters, seconds, degrees Kelvin, and calories/mole.

a) Third body efficiencies are: CH_4 : 6.5, H_2O : 6.5, CO_2 : 1.5, H_2 : 1.0, CO : 0.75, O_2 : 0.4, N_2 : 0.4, all other species: 1.0.

b) High pressure value k_∞. The pressure dependence is given by the Lindemann form $k = k_\infty/(1 + (\alpha RT/p))$, where $\alpha R = 0.517 \exp(-9000/T)$, with p in atm and T in degrees Kelvin.

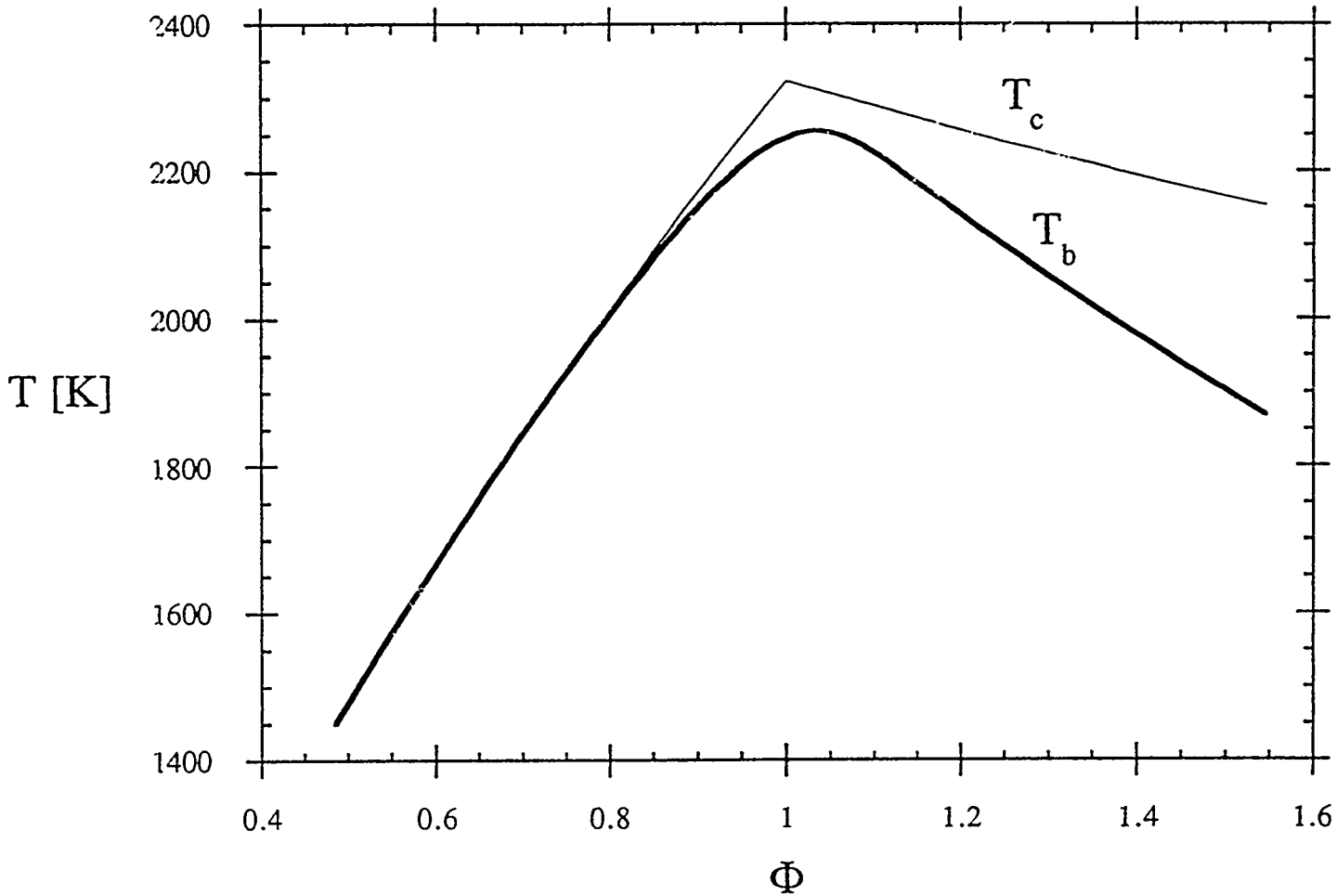

Fig. 1a

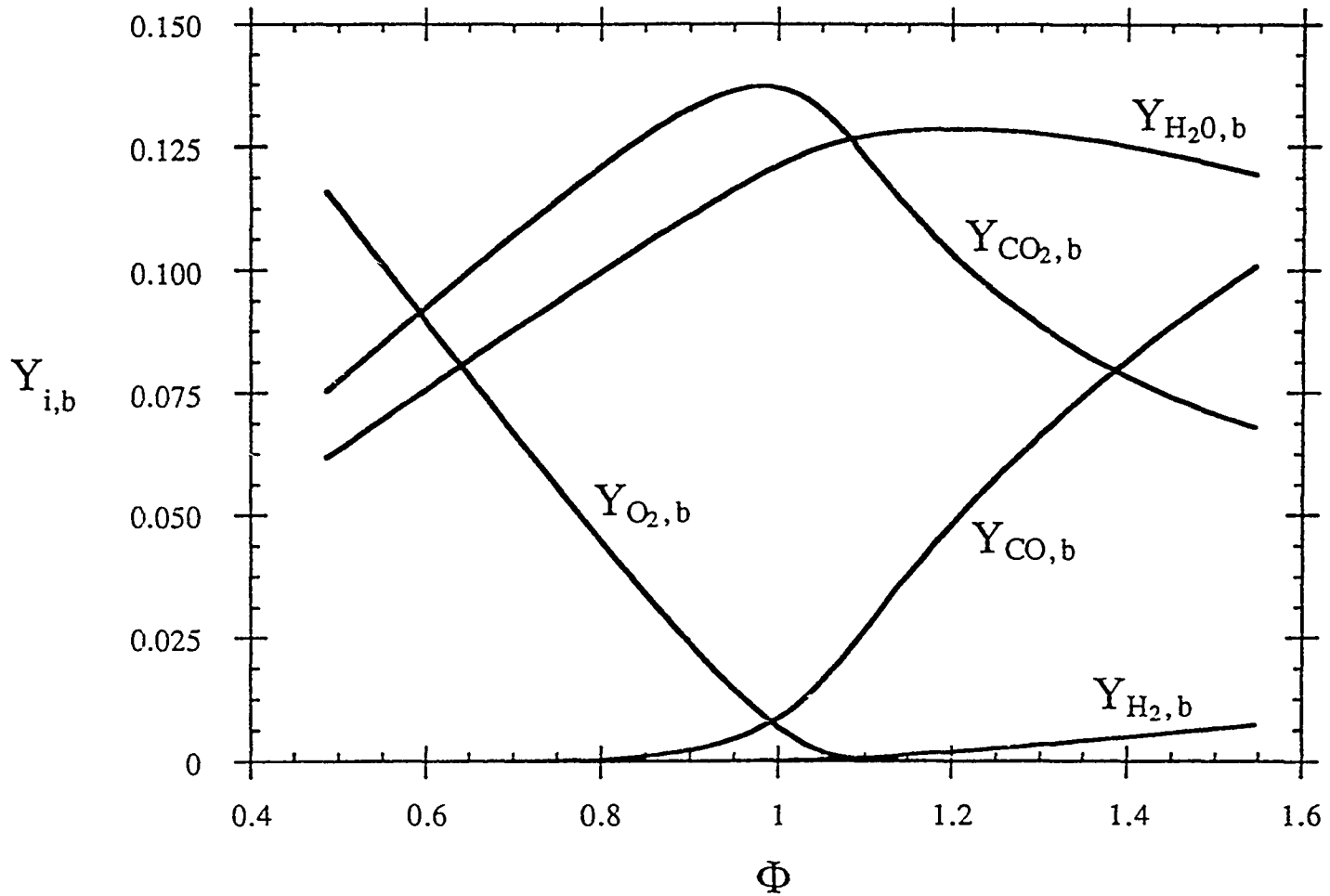
0.150
0.125
0.100
0.075
0.050
0.025
0
$Y_{i,b}$
0.4
0.6
0.8
1
1.2
1.4
1.6
Φ
$Y_{H_2O,b}$
$Y_{CO_2,b}$
$Y_{O_2,b}$
$Y_{CO,b}$
$Y_{H_2,b}$

Fig 16

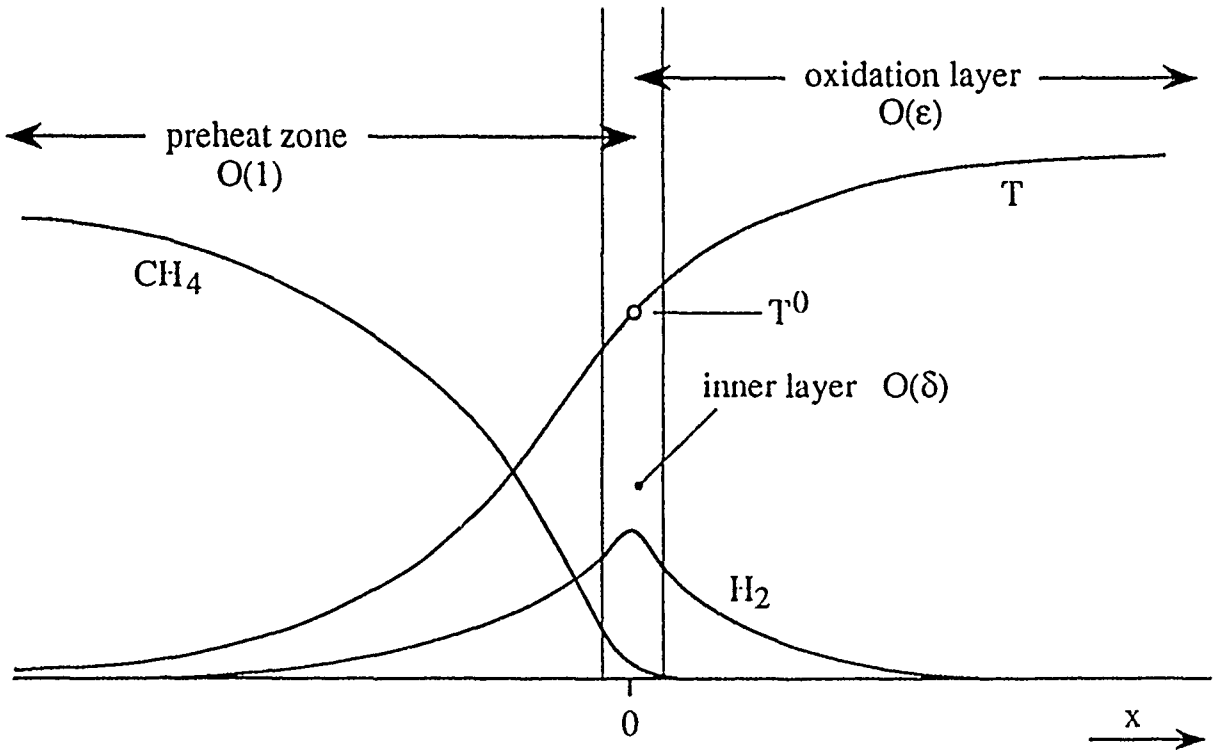
oxidation layer
O(ε)
preheat zone
O(1)
T
CH4
T^0
inner layer O(δ)
H2
0
x

Fig. 2

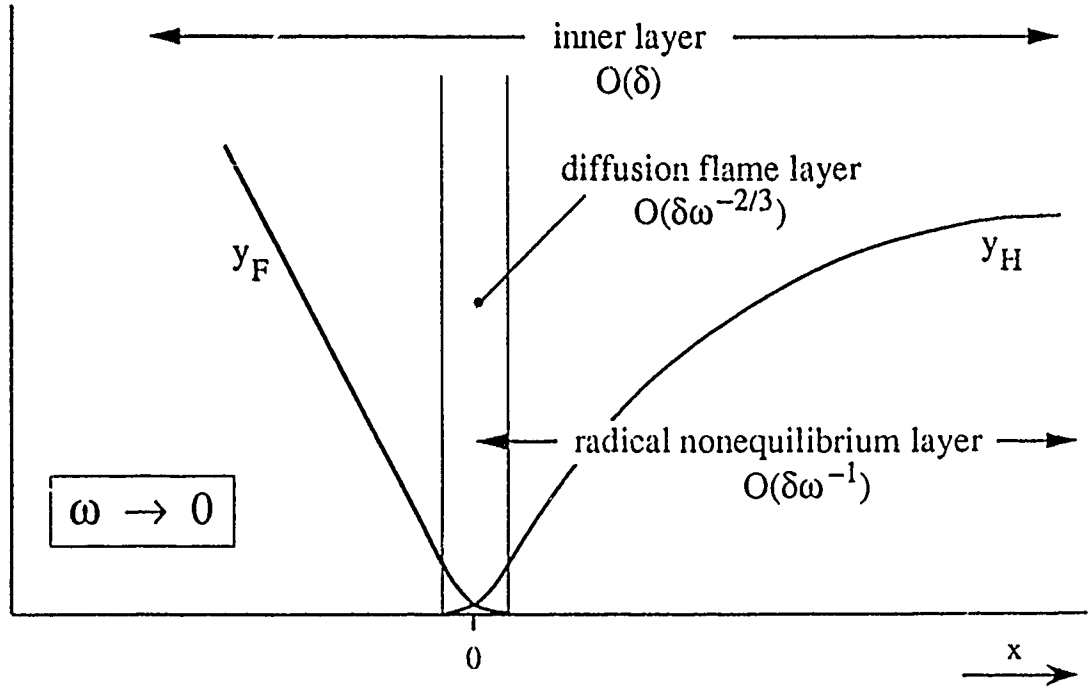
inner layer
O(δ)
diffusion flame layer
O(δω^-2/3)
y_F
y_H
radical nonequilibrium layer
O(δω^-1)
ω → 0
0
x

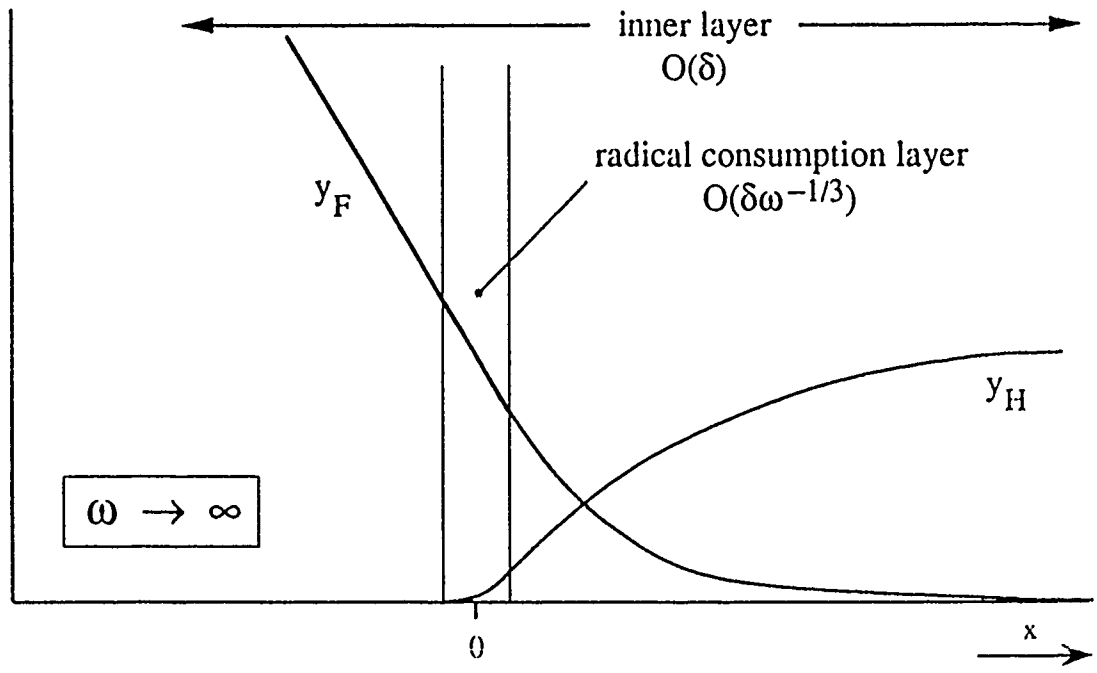
inner layer
O(δ)
radical consumption layer
O(δω^-1/3)
y_F
y_H
ω → ∞
0
x

Fig. 3

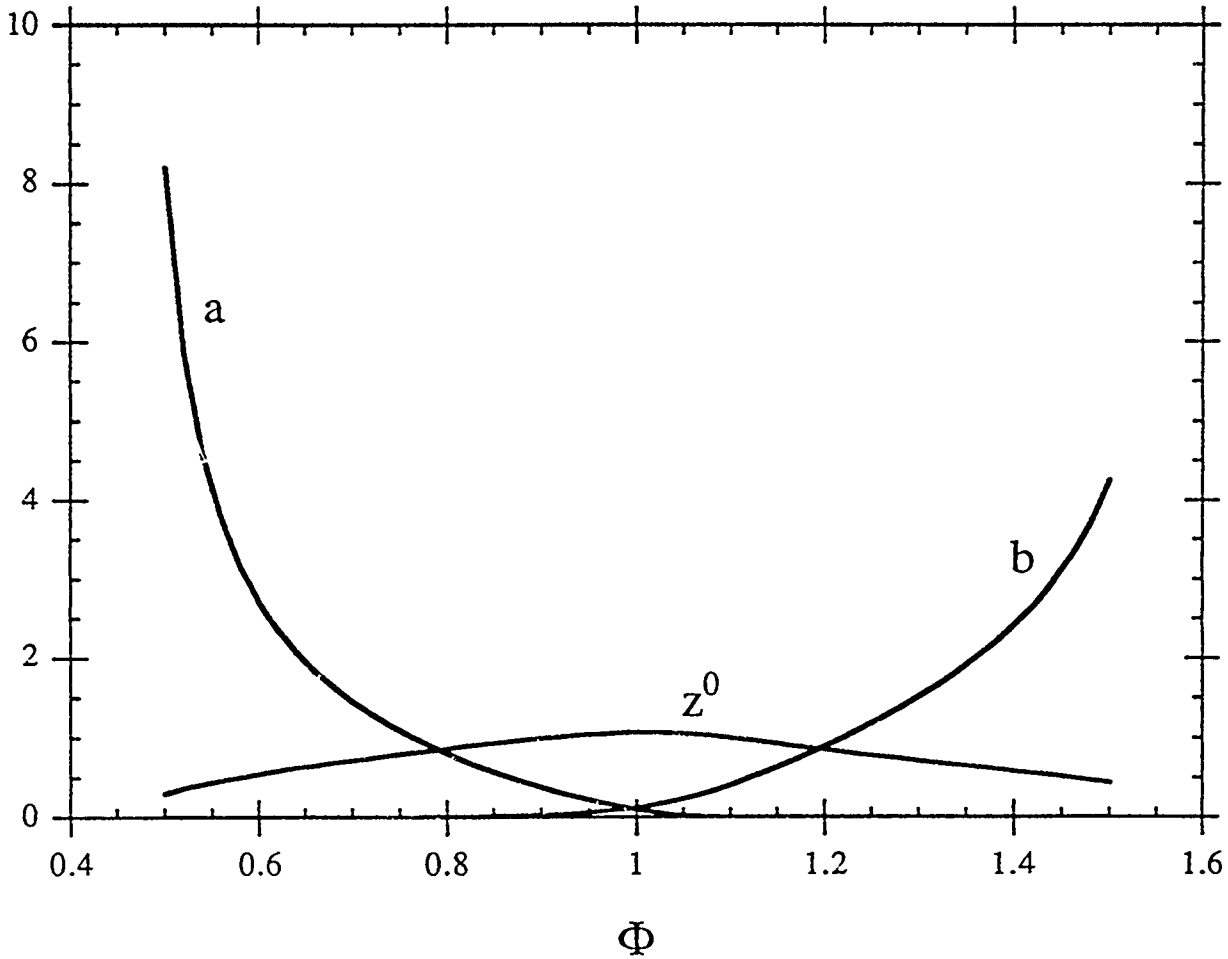

Gk

Fig. 6

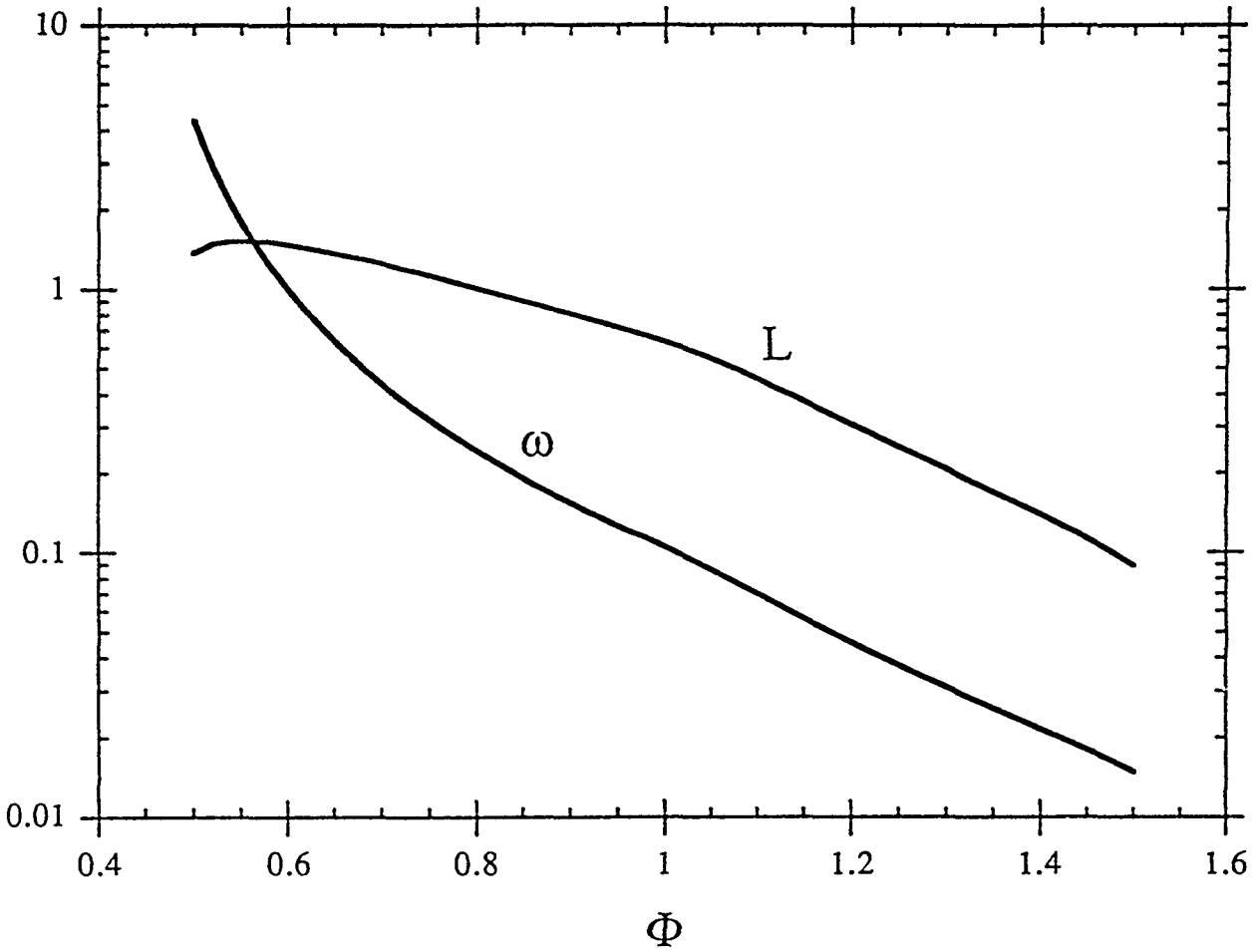

Fig. 5

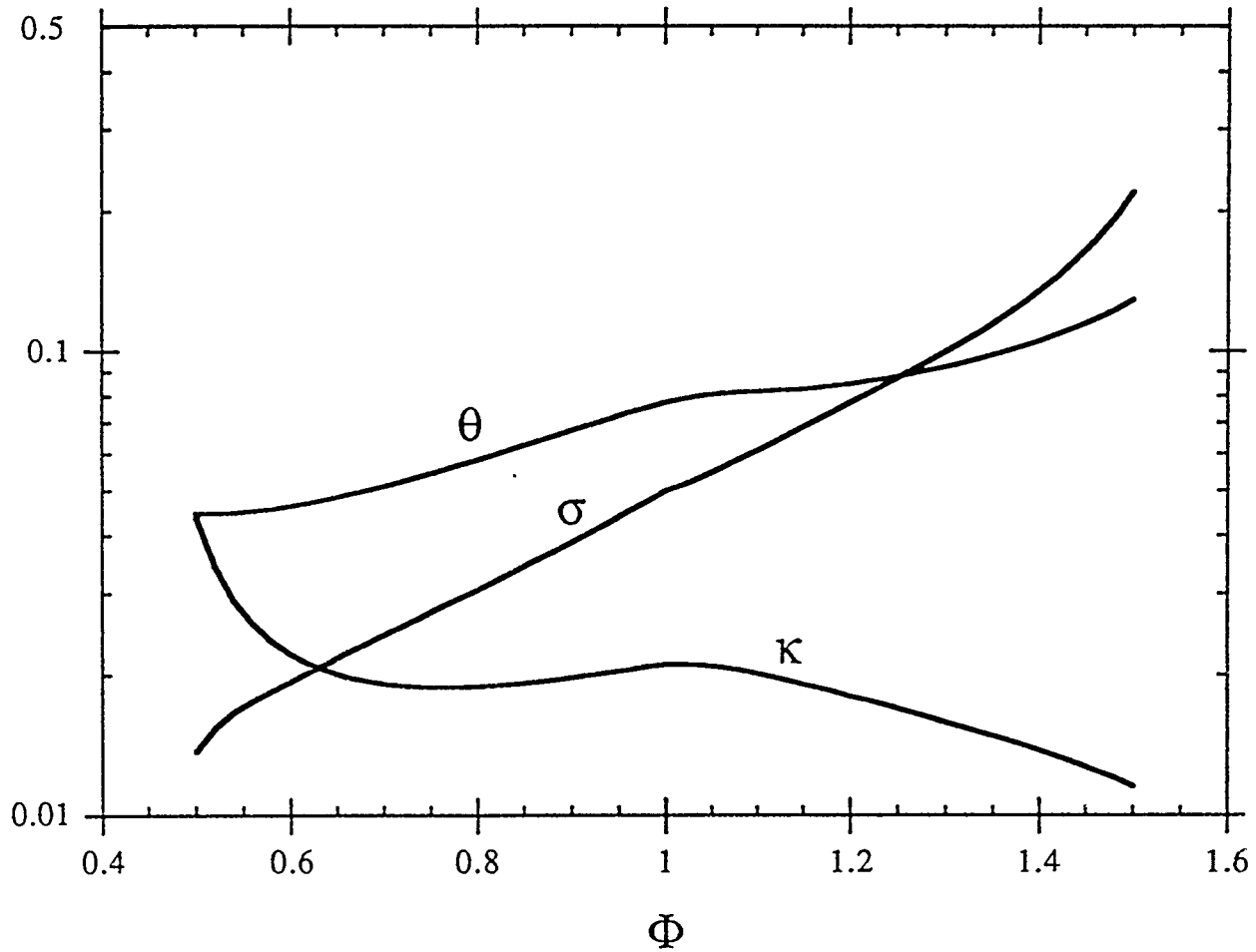

Fig. 6

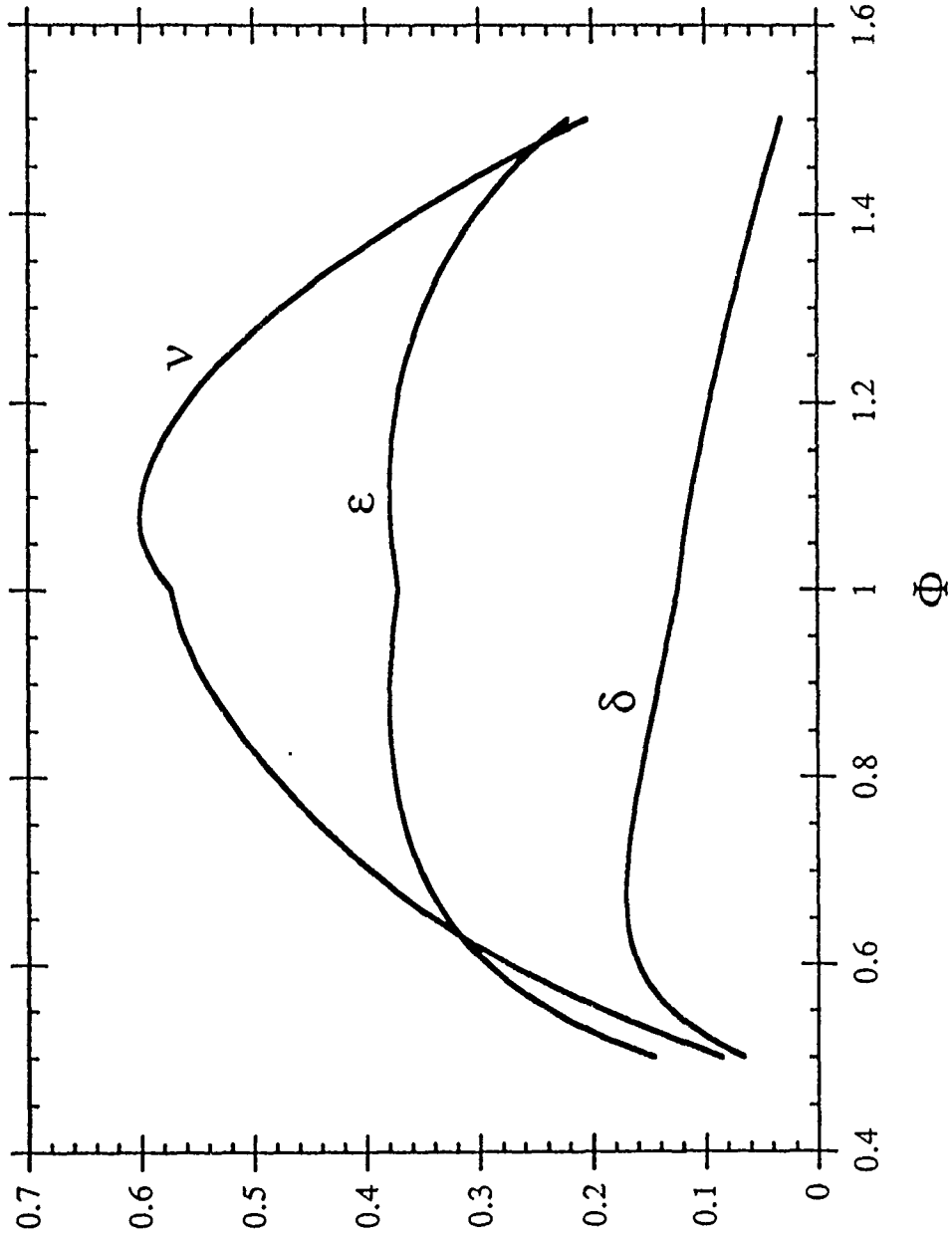

Fig. 2

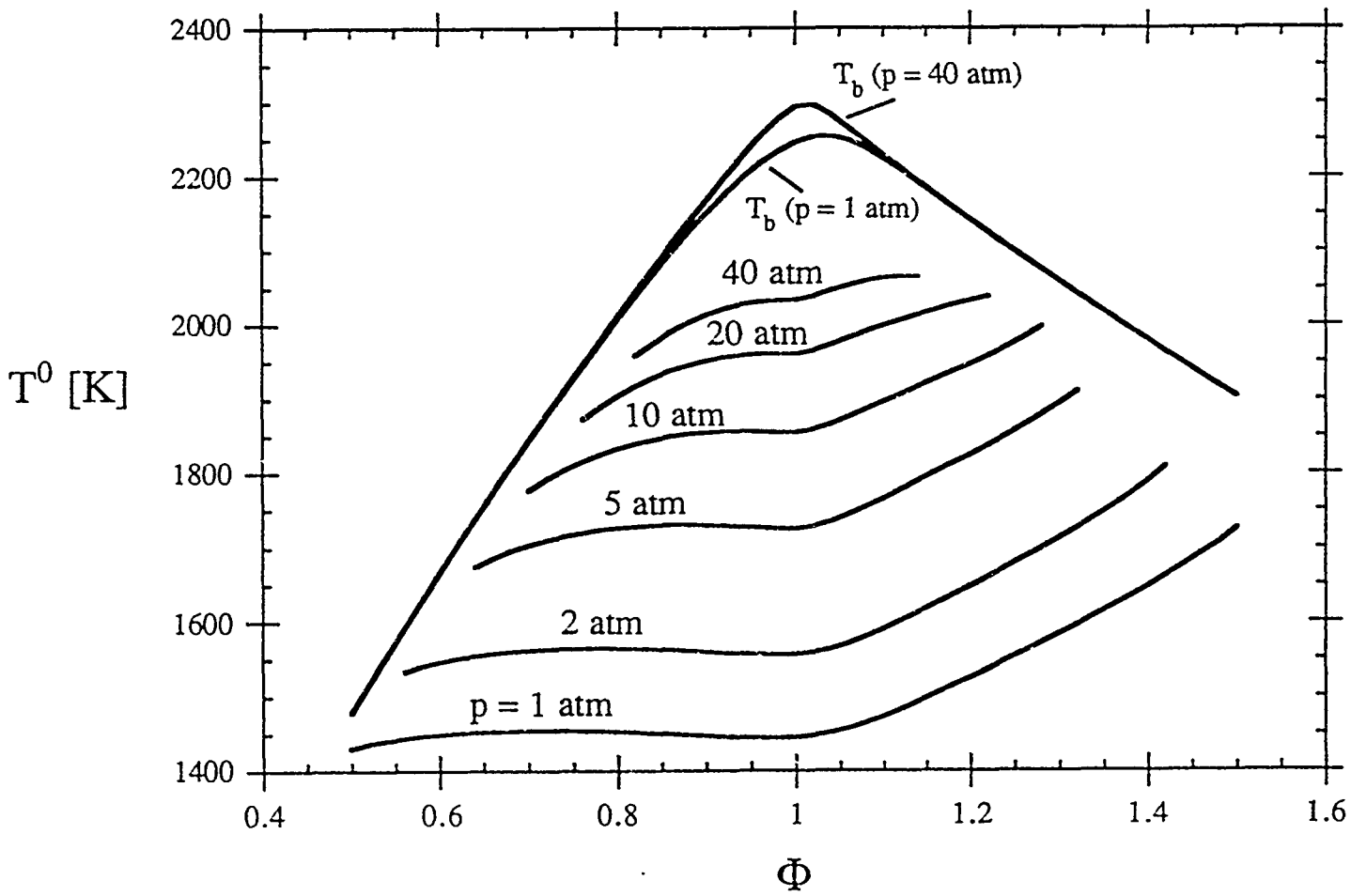
2400
2200
2000
1800
1600
1400
T^0 [K]
0.4
0.6
0.8
1
1.2
1.4
1.6
Φ
T_b (p = 40 atm)
T_b (p = 1 atm)
40 atm
20 atm
10 atm
5 atm
2 atm
p = 1 atm

Fig. 2

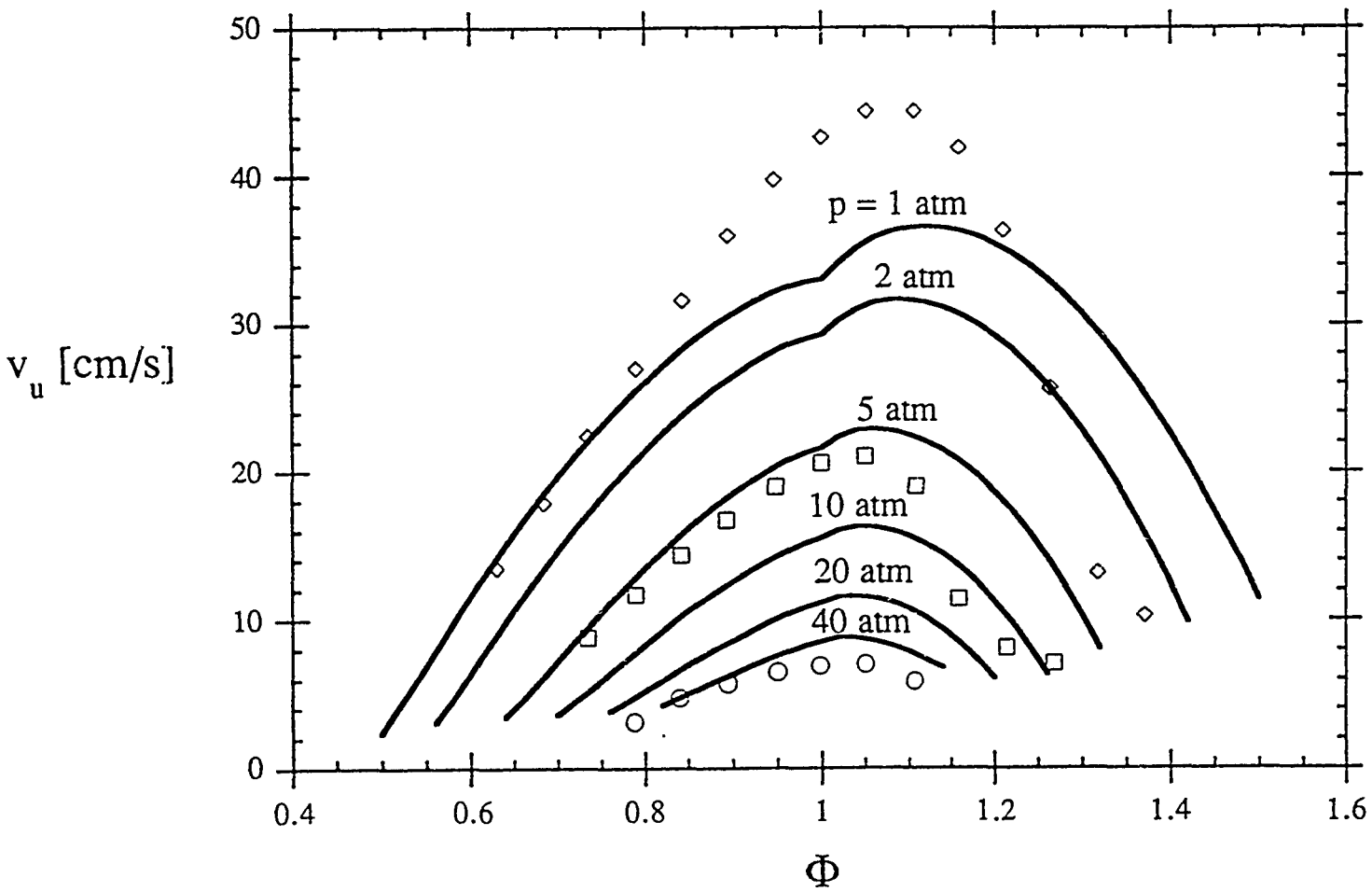
50
40
30
20
10
0
0.4
0.6
0.8
1
1.2
1.4
1.6
p = 1 atm
2 atm
5 atm
10 atm
20 atm
40 atm
v_u [cm/s]
Φ

Fig. 5

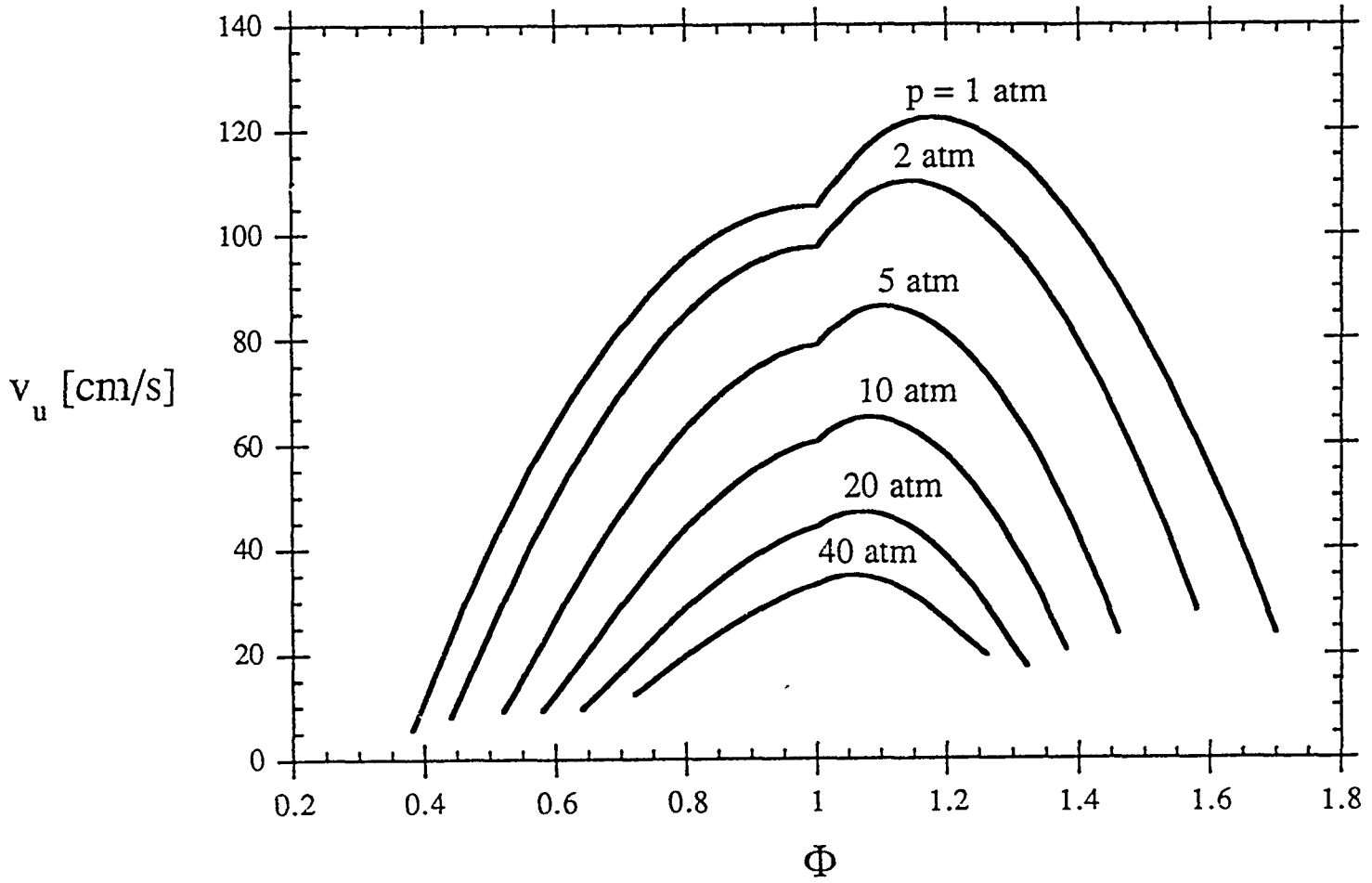
140
120
100
80
60
40
20
0
0.2
0.4
0.6
0.8
1
1.2
1.4
1.6
1.8
p = 1 atm
2 atm
5 atm
10 atm
20 atm
40 atm
v_u [cm/s]
Φ

Fig. 10

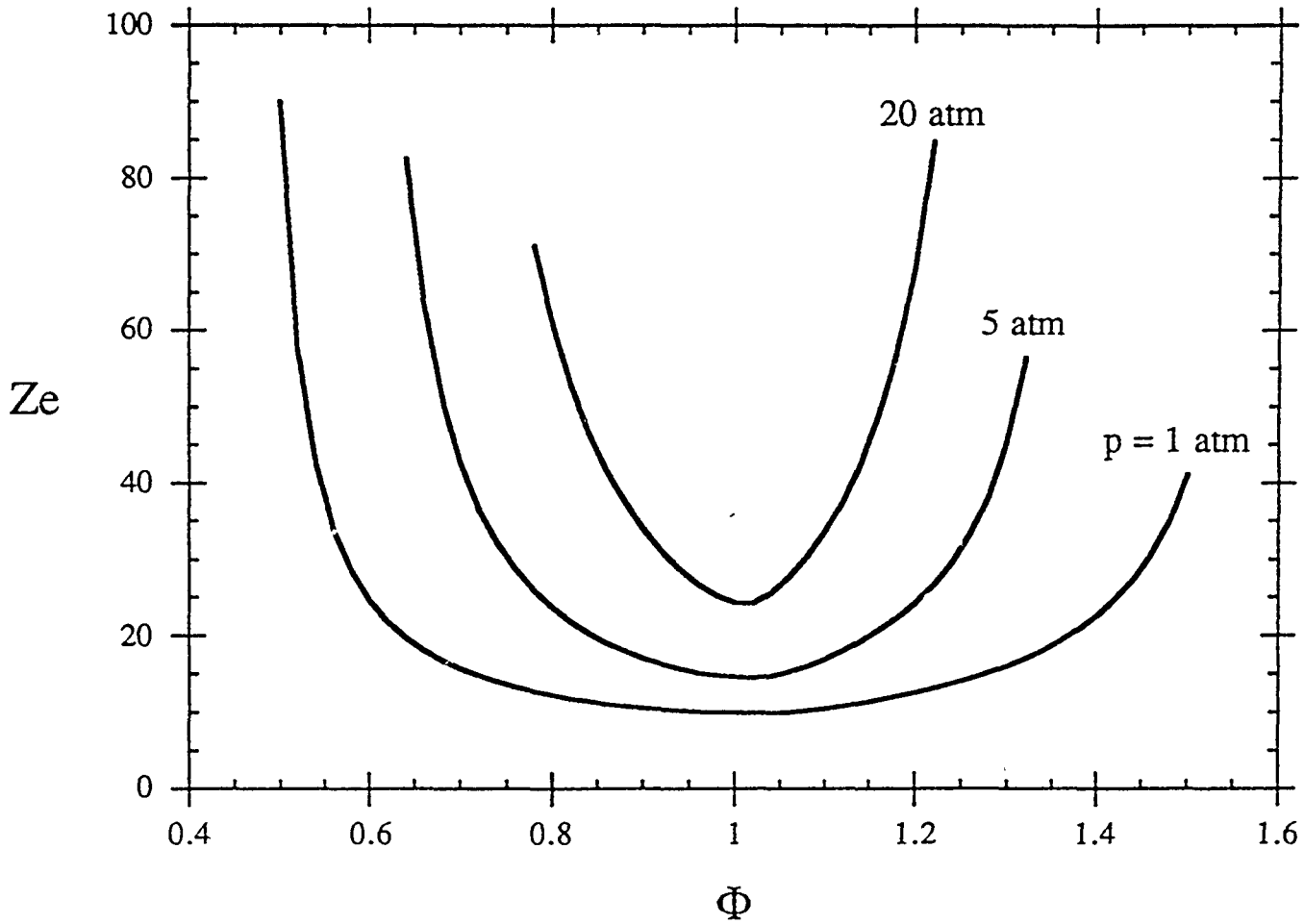

Fig. 11

CHAPTER VI.

THE STRUCTURE AND EXTINCTION OF PARTIALLY PREMIXED FLAMES BURNING METHANE IN AIR

It was mentioned in chapter II that turbulent reacting flows can be modelled as a statistical ensemble of laminar diffusion flamelets, laminar premixed flamelets, and laminar partially premixed flamelets. These flamelets are subjected to strain. In chapters III and IV the structure of diffusion flamelets were considered, while in chapter V the structure of premixed flamelets were considered. To complete the description of laminar flamelets, in this chapter laminar partially premixed flamelets are considered. As in chapters III, IV and V, methane is used as the model hydrocarbon fuel. A experimental and numerical study of the structure and mechanisms of extinction of counterflow, partially premixed, flames burning methane was performed. Experimental data was obtained for the temperature profile, the axial velocity profile, the concentration profiles for various stable species and the critical conditions of the flame at extinction. The results WEre compared with numerical calculations performed at conditions identical to those used in the experiment. Experimental measurements and numerical calculations show that the partial premixing of the reactant streams of a counterflow diffusion flame makes the flame less resistant to stretch. In addition, numerical calculations show that the reaction zone of a partially premixed flame exhibits a diffusion flame and a premixed flame-like structure. Both results are consistent with previous asymptotic analyses of the structure of partially premixed flames.

The research summarized above has been published in the Proceedings of the Twenty-Second Symposium (International) on Combustion, The Combustion Institute, pp 1555-1563, 1988. The coauthors of this manuscript are Professor M. D. Smooke, and Dr. I. K. Puri. The research performed by Professor M. D. Smooke at Yale University was supported by the Office of Naval Research.

CHAPTER VII. HYDROGEN-AIR DIFFUSION FLAMES

VII.1 ANALYSIS OF THE STRUCTURE OF COUNTERFLOW HYDROGEN-AIR DIFFUSION FLAMES.

Numerical calculations and asymptotic analysis of the structure of hydrocarbon flames described in chapters II - VI show that the structure of the oxidation layer in these flames are primarily determined by H_2-O_2 reactions. Hence, to obtain an improved understanding of the structure of the oxidation layer in hydrocarbon flames, numerical calculations were performed to determine the structure of diffusion flames stabilized between counterflowing, laminar streams of hydrogen and air. The calculations were performed at different values of the rate of strain and at a value of the absolute pressure equal to one atmosphere. The detailed kinetics of oxidation of hydrogen was represented by eleven elementary reactions involving seven species. Temperature profiles, concentration profiles of various stable species and radicals, rates of various elementary chemical reactions, and rates of formation of various species and radicals were calculated for a number of values of the rate of strain. Results are plotted at a low value of the rate of strain (= 30 s^{-1}) and at a high value of the rate of strain (= 1440 s^{-1}). At the low value of the rate of strain, a number of reactions were found to be in partial equilibrium over a major part of the flow field. Using approximations suggested by the results of the numerical calculations, the equilibrium structure of the flame was determined and the results were compared with the results of numerical calculations performed at a value of the rate of strain equal to = 30 s^{-1} and good agreement was obtained for the concentration profiles of H_2, O_2, H_2O, and H. However the shapes of the temperature profiles were different and they are attributed to nonequilibrium of the major chain branching reaction $H + O_2 = OH + O$. This study shows that a number of approximations employed in chapters I - VI in describing the structure of the oxidation layer of hydrocarbon air flames are reasonably accurate.

The research summarized above has been accepted for publication in Progress in Astronautics and Aeronautics, 1990. The coauthors of the publication are Dr. Venkat Tangirala, Professor C. Trevino, and Professor M. D. Smooke.

VII.2 THE INFLUENCE OF THE LEWIS NUMBER OF THE REACTANTS ON THE ASYMPTOTIC STRUCTURE OF COUNTERFLOW AND STAGNANT DIFFUSION FLAMES

In the asymptotic analysis described in chapter VII.1, the Lewis number for all species were presumed to be unity. However, for hydrogen the characteristic Lewis number is small. Hence, in this section the asymptotic structure of counterflow and stagnant diffusion flames are analyzed in the limit for large values of the overall, nondimensional activation energy, T_a, characterizing the rate of the reaction, and results are given for small values of the stoichiometric fuel to oxygen mass ratio. The chemical reaction between the fuel and the oxidizer is represented by a one-step, irreversible process. A new approach is developed to characterize the influence of the Lewis number of the fuel, L_F, and the Lewis number of the oxidizer, L_O, on the outer and the inner structure of near equilibrium diffusion flames. Explicit algebraic formulas to predict the critical conditions of flame extinction are also given.

For counterflow diffusion flames at fixed values of L_O, the flame moves significantly toward the oxidizer stream, and the heat losses toward the oxidizer region of the flame increases significantly with decreasing values of L_F. The value of the maximum flame temperature is relatively insensitive to the variations in L_F although the value of the rate of strain at extinction, A, increases significantly with decreasing values L_F and increasing values of T_a. At fixed values of L_F and decreasing values of L_O, the flame moves slightly toward the fuel stream; the heat losses toward the fuel stream increases slightly, and there is moderate increase in the value of the maximum flame temperature. The value of A increases with decreasing values of L_O for large values of T_a and is relatively insensitive to variations in L_O for moderate values of T_a.

The inner and outer structure for stagnant diffusion flames where convection is absent are qualitatively similar to those for counterflow diffusion flames. However, the value of the maximum flame temperature increases significantly with decreasing values of L_O and fixed values of L_F.

The results developed here are used to obtain overall chemical kinetic rate parameters characterizing the gas phase oxidation of methane using previously measured values of the critical conditions of flame extinction.

The research summarized above has been published in Combustion Science and Technology, Volume 64, pp 243-261, 1989 The coauthor of this publication is Professor C. Trevino.